In presenting the dissertation as a partial fulfillment of the requirements for an advanced degree from the Georgia Institute of Technology, I agree that the Library of the Institute shall make it available for inspection and circulation in accordance with its regulations governing materials of this type. I agree that permission to copy from, or to publish from, this dissertation may be granted by the professor under whose direction it was written, or, in his absence, by the Dean of the Graduate Division when such copying or publication is solely for scholarly purposes and does not involve potential financial gain. It is understood that any copying from, or publication of, this dissertation which involves potential financial gain will not be allowed without written permission.

_____

_____

3/17/65
b

THE DIFFUSION OF CHLORINE INTO THE DURANGO, MEXICO FLUORAPATITE

A THESIS

Presented to

The Faculty of the Graduate Division

by

Eugene Corry Clark

In Partial Fulfillment

of the Requirements for the Degree

Master of Science in Ceramic Engineering

Georgia Institute of Technology

June, 1968

THE DIFFUSION OF CHLORINE INTO

THE DURANGO, MEXICO

FLUORAPATITE

Approved:

Chairman

Date approved by Chairman: March 6, 1968

ACKNOWLEDGMENTS

I wish to express my appreciation to my wife for her patience and understanding throughout this work, and I wish to recognize the many sacrificies she has made in my behalf.

I wish to thank Dr. W. E. Moody for acquainting me with the problem and for his extremely valuable constructive criticism and guidance throughout the experiment.

I wish to thank the other members of my Committee for their assistance.

I wish to thank Mr. Thomas Mackrovitch for his assistance in fabricating the apparatus used in the experiment. I wish to thank Miss Jane Thacker for the typing of the rough draft.

TABLE OF CONTENTS

TABLE OF CONTENTS (Continued)

LIST OF TABLES

LIST OF TABLES (Continued)

LIST OF TABLES (Continued)

LIST OF ILLUSTRATIONS

SUMMARY

To understand more about anion movement through apatites, the diffusion rates and activation energies of chlorine in the Durango, Mexico Fluorapatite were experimentally determined.

The samples were exposed to a NaCl vapor at temperatures from 900°C to 1300°C and were allowed to cool to room temperature. Electron microprobe scans were made of the chlorine penetration in the directions perpendicular and parallel to the c-axis. A model mathematical function was fitted to the electron probe chlorine intensities by a least square method, and the fitted mathematical model parameter was used to calculate the diffusion coefficients.

The technique of fitting a model mathematical function to the electron probe data appeared to work reasonably well. The calculated diffusion coefficients for chlorine diffusion parallel and perpendicular to the c-axis ranged from 10^{-13} to 10^{-10} cm.^{2}/sec. and from 10^{-14} to 10^{-11} cm.^{2}/sec. respectively. The calculated chlorine activation energies for diffusion parallel and perpendicular to the c-axis were 2.1 ± .6 e.v. and 1.7 ± .8 e.v. respectively. The calculated diffusion constants for chlorine diffusion parallel and perpendicular to the c-axis were $3.22 \cdot 10^{-4}$ cm.^{2}/sec. and $2.07 \cdot 10^{-6}$ cm.^{2}/sec. respectively.

The suggested mechanism for the diffusion of chlorine is a vacancy-atom mechanism. Probably there were some short circuit diffusion paths present perpendicular to the c-axis, as the diffusion constant was relatively small for diffusion in that direction. The lack of a

significant difference between the two activation energies suggest that the chlorine movement down the calcium triangle columns parallel to the c-axis was restricted by the fluorine in the calcium columns.

CHAPTER I

INTRODUCTION

Bone and teeth are composed of inorganic and organic phases. The inorganic phase is considered to be the hydroxyapatite mineral, $Ca_{10}(PO_4)_3(OH)_2$. The role of apatite in bone and tooth growth, as well as tooth decay, is still largely unknown. The exchangeability of the anions, $(OH)^-$, F^-, and Cl^-, and their relation to the apatite structure may be very important. Fossil bone and teeth have been found to have much of the $(OH)^-$ ions replaced by the F^- ion, and this replacement is thought to enable the fossils to survive time's ravages. Apatites with the $(OH)^-$ ion replaced by the Cl^- ion are found to occur naturally. The $(OH)^-$, F^-, and Cl^- ions are commonly found in the human body chemistry, but the replacement of $(OH)^-$ by Cl^- or F^- is believed to be uncommon in human bone or tooth apatite.

A better understanding of the replacement process would enable an estimate to be made of the influence of anions in bone and tooth mineral structure and chemistry, as well as other biological implications. Any anion replacement will probably be a diffusion controlled process, and it is desirable that activation energies for different possible anion-apatite combinations be found.

A step in the achievement of anion-apatite activation energy data is the determination of the activation energy of the chlorine ion into a naturally occurring fluorapatite, the Durango, Mexico Fluorapatite.

CHAPTER II

REVIEW OF THE LITERATURE

Chlorine Ion

The chlorine ion is a negatively and singularly charged atom with an ionic radius of 1.81 angstroms, and it is larger than the fluorine ion with an ionic radius of 1.36 angstroms and the hydroxyl ion which has an effective ionic radius of 1.53 angstroms according to Evans (1). The fluorine and hydroxyl ions, like chlorine ions, have a single negative charge. Chlorine and fluorine ions may be thought of as essentially spheres where as a pear shape might better describe a hydroxyl ion. The hydroxyl ion has a dipole character, but the chlorine and fluorine ions do not have this characteristic property.

Structure of Apatites

Basic Apatite Structure

Posner, Perloff, and Diorio (2) reported that hydroxyapatite had a space group of $P6_3/m$ and axis lengths of a = b = 9.432 and c = 6.881 angstroms. Kay, Young, and Posner (3) using neutron diffraction data and more precise x-ray data, resolved the structure to that as shown in Figure 1. The location of the hydrogen was established from the neutron diffraction data. In Figure 2 from Kay, et al., it can be seen how the hydroxyl ions are not centered in the tri-calcium plane. Fluorine was an impurity in the sample used and its location is centered in the calcium plane. Normally the hydrogen ion of the hydroxyl will point up or down,

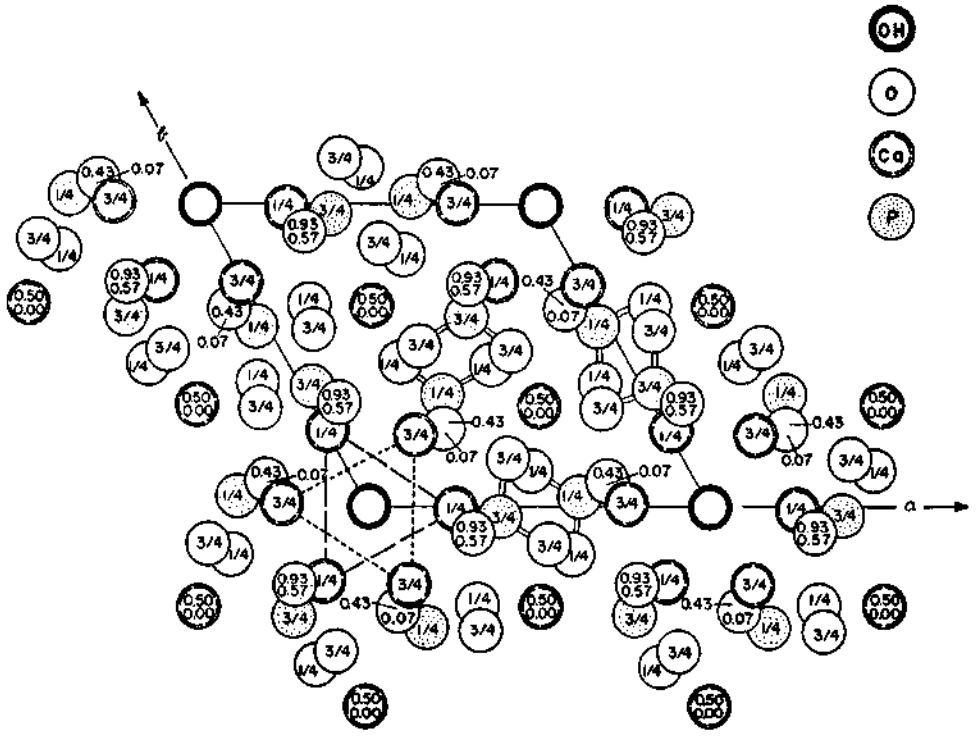

Figure 1. Hydroxyapatite Structure.

The structure is projected onto the x,y plane, and the numbers written in the symbols are the z parameters. The dashed and dotted lines outline the calcium triangles at z = 1/4 and z = 3/4, respectively. Two of the O's in each PO_4 tetrahedra are superimposed and partially overlap the P in this projection. In some of the tetrahedra the two remaining P-O bonds are indicated by parallel lines, ═══ .

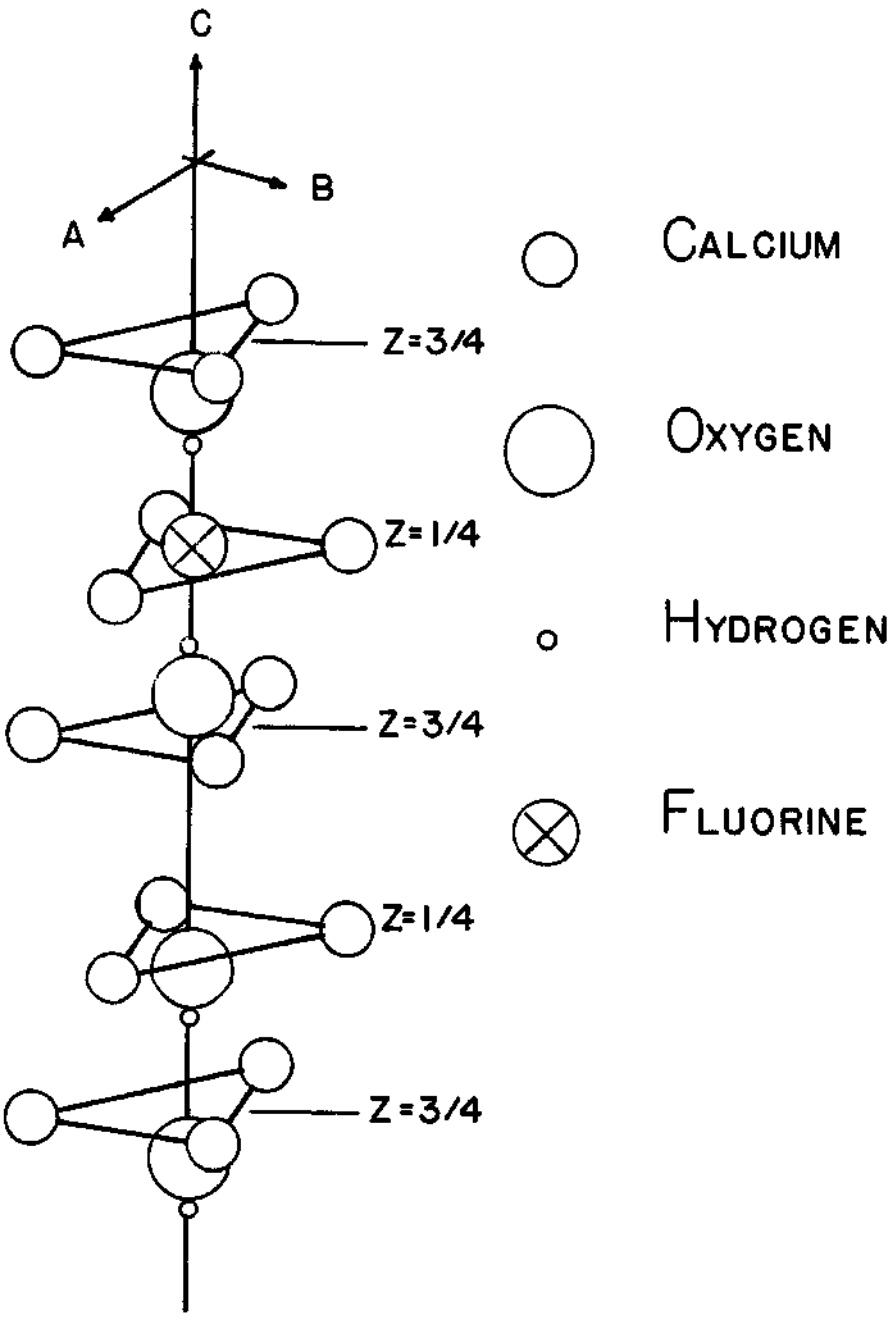

Figure 2. Perspective View of the Calcium Triangle Arrangements. (Calcium triangle locations are given in terms of the z parameter.)

but if an impurity is present the order is interrupted. If a fluorine ion is present, the hydrogen will point towards the fluorine ion, thus disturbing the ordering of the hydroxyl ions. Kay, et al. found that the hydroxyl ion's thermal vibrations were much larger in a direction parallel to the c-axis (up and down the calcium triangle columns) than perpendicular to the c-axis. Some rocking of the hydrogen was found to exist. The freedom of the hydroxyl ion to move about suggests a relatively open nature of the structure in the column.

Young and Elliott (4) report that the fluorine is centered in the calcium triangle plane and other than a small amount of shifting of the atoms to accommodate the fluorine, fluorapatite is little different from hydroxyapatite. Young and Elliott (4) report in Table 1 that the fluorapatite a-axis length is somewhat less than the hydroxyapatite and c-axis is very slightly less than hydroxyapatite. It is thought that the fluorine has a strong attraction for the three calciums around it, which causes the calcium triangle to become more compact. The end result is that the a-axis is shorter with respect to the hydroxyapatite.

Table 1. Apatite Lattice Parameters

Apatite	a(A) Est. Error	c(A) Est. Error	Unit Cell Volume (A)
Fluorapatite	9.364 (0.005)	6.879 (0.005)	521.3
Hydroxyapatite	9.422 (0.003)	6.883 (0.003)	529.2
Chlorapatite	9.634*(0.005)	6.783 (0.005)	545.2

*Actually b and a/2 in the $P2_1/a$ space group.

Young and Elliott (4) report that in chlorapatite the tri-calcium triangles are larger and that the chlorine ion is located above the calcium plane nearly half the distance to the next calcium triangle plane. In Table 1 the a-axis length of chlorapatite is quite larger than that of the hydroxyapatite. The negative ions near the middle of two calcium triangle layers would tend to draw them closer together as seen by the shorter c-axis length of the chlorapatite with respect to hydroxyapatite. The chlorine ion is much larger than the fluorine or hydroxyl ion and needs more room. The anion is accommodated by the calcium triangles extending themselves and the anions shifting into the space between triangles. The progressive shift of axis lengths as different anions are placed in the column positions can be seen in Figure 3, Young and Elliott (4).

The displacement of the chlorine ion from the center of the calcium triangle is very similar to that of hydroxyapatite and in Figure 4, Young and Elliott (4), the positions are shown. The exact location of the chlorine ion does not lie in the center but closer to one plane than the other.

Young and Elliott (4) report that very pure synthetic chlorapatite is monoclinic. A phase change occurs below 500°C., and it is suggested that the new phase is hexagonal. Furthermore, the phase change appears to be a reversible one. They report that small amounts of impurities such as hydroxyl ions and other atoms will stabilize the apatite in the hexagonal form. It is further suggested that in all of the natural specimens the impurity content is sufficiently large to stabilize the chlorapatite in the hexagonal form. In the monoclinic form the b-axis

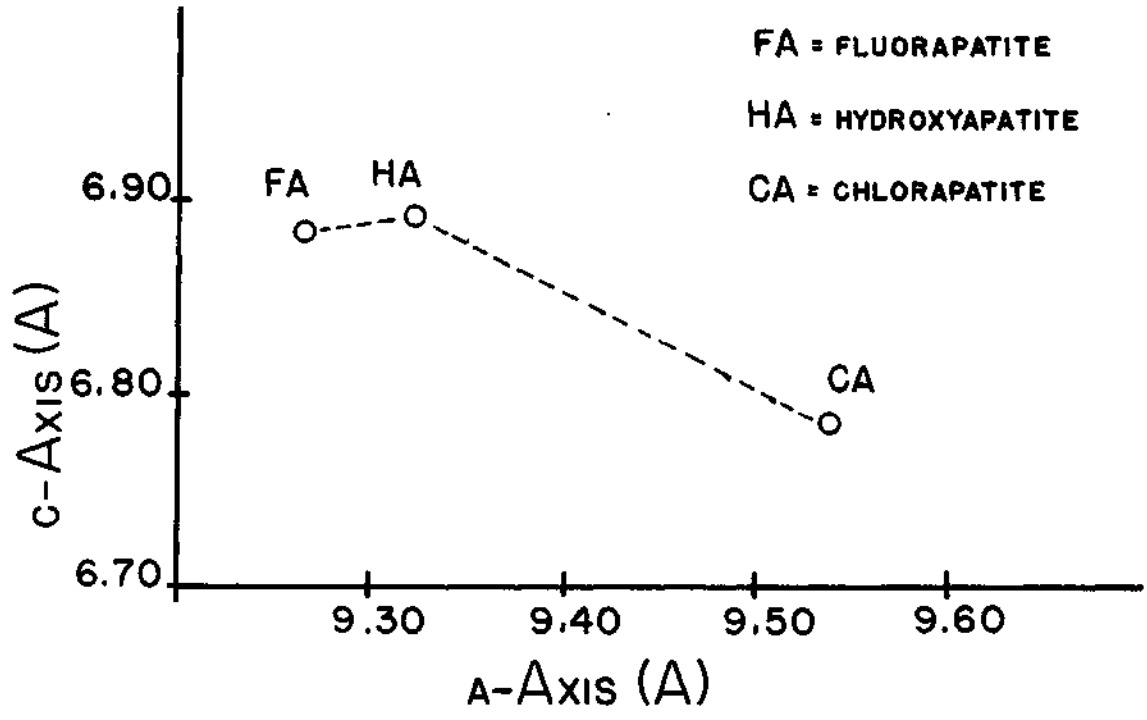

Figure 3. Relationships Between the Lattice Parameters.

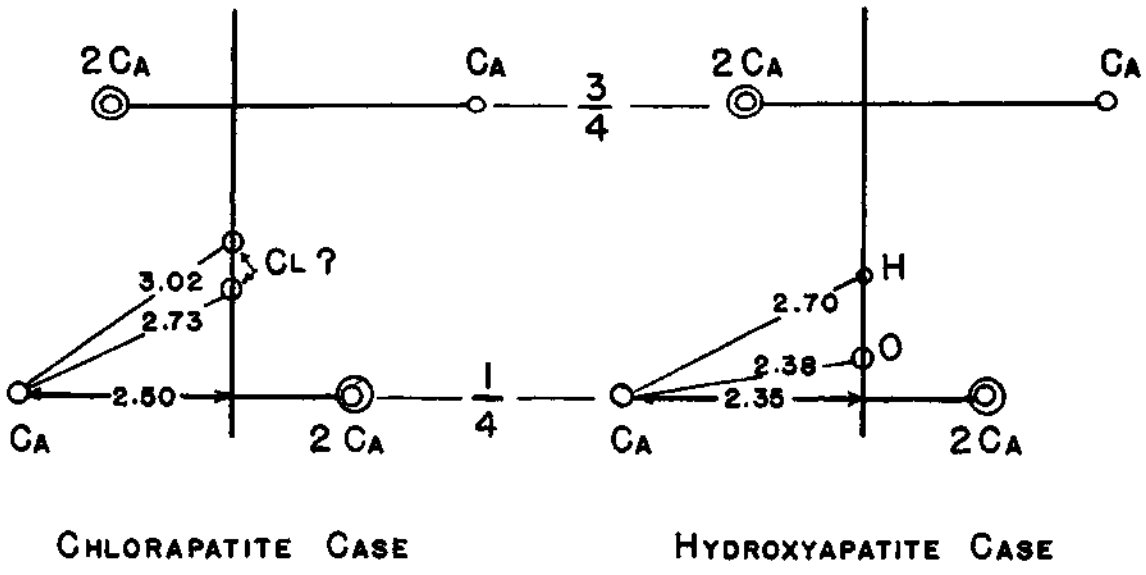

Figure 4. Geometric Relationships of Various Ions to Calcium Triangles. (Distances in Angstroms)

equals one half the a-axis length. The change may be interpreted as a transformation of the chlorine ion from an ordered dipole arrangement to a statistically disordered arrangement.

Durango, Mexico Fluorapatite

Durango Fluorapatite crystals are relatively large, clear yellow-green crystals, having a well developed morphology. The average size is approximately three centimeters long and from one to two centimeters in diameter. Incomplete chemical analysis made by Trautz (5) and Baddiel and Berry (6) are given in Table 2 along with theoretical fluorapatite values. Bhimasenacher (7) reported a density of 3.218 grams per cubic centimeter for Durango Fluorapatite. Trautz (5) and Carlstrom (8) made determinations of the Durango, Mexico Fluorapatite lattice parameters, which are given in Table 3. Larsen and Berman (9) reported the indices of refraction for fluorapatite as: the extraordinary ray, 1.630 and the ordinary ray, 1.633; and they report the density to be 3.2 grams per cubic centimeter.

In Baddiel and Berry's (6) infrared study of a hydroxyapatite and the Durango, Mexico Fluorapatite they found the PO_4^{3-} ions to appear to exist as tetrahedral units with weak bonds with other ions. In general, the complete structure appeared very open and of a low packing density.

Hydroxy-Fluor-Chlor-Apatite Conversion

Probably the first successful conversion of one form of apatite to another was achieved by Schleede, Meppen, and Jorgensen (10), when they converted a natural fluorapatite into a hydroxyapatite by heating the sample to 1360°C in a steam atmosphere. Later Wallaeys (11) was able to

Table 2. A Partial Chemical Analysis of Durango, Mexico Fluorapatite

References	Ca/P Ratio*	Ca/F Ratio	F%**	CO_2%	SO_4^{-2}	NO_3^{-1}
Trautz (5)	1.688	5.883	3.21	0.24	-	-
Baddiel, et al.(6)	1.667	5.05	-	0.1	Nil	Nil
Theoretical	1.666	5.00	3.77	-	-	-

*molar ratio.

**per cent by weight.

Table 3. Durango Mexico Fluorapatite Crystal Axis Lengths

Reference	a-axis (Angstroms)	c-axis (Angstroms)
Trautz (5)	9.387 ± .003	6.880 ± .002
Carlstrom (8)	9.391 ± .001	6.874 ± .001
Theoretical* Pure Synthetic	9.373 ± .003	6.882 ± .003
Theoretical** Synthetic	9.370 ± .001	6.884 ± .001

*Values from a pure synthetic fluorapatite prepared by Trautz (5).

**Values from synthetic fluorapatite prepared by Carlstrom (8).

convert chlorapatite to hydroxyapatite, hydroxyapatite to chlorapatite, and hydroxyapatite to fluorapatite. Conversions to a hydroxyapatite were accomplished with a steam atmosphere at about 800°C. Other conversions were accomplished by heating the base apatite with a calcium salt of the desired ion to about 800°C. Elliott and Young (12) took single crystals of chlorapatite and converted them to hydroxyapatite by heating the samples to 1300°C in a steam atmosphere. Breitmoser and Young (13) report that an attempt to convert a single crystal of fluorapatite at 1200°C in a steam atmosphere was not successful.

It is not unusual to find fossilized bone where there has been a conversion of the hydroxyapatite to fluorapatite (4), suggesting that fluorine will replace the hydroxyl ion at low temperatures over a long time span.

Theory of Diffusion

Diffusion processes are functions with many independent parameters such as time, temperature, solute concentration, solvent structure, and solvent imperfections as well as the intrinsic properties of the solute and solvent. The development of Fick's laws is given by Barrer (14) and Crank (15) with solutions for specific experimental conditions. The most useful of Fick's Laws is the second law:

$$dc/dt = \frac{d(D \frac{dc}{dx})}{dx} \qquad (1)$$

where: dc/dt = change in concentration with time

dc/dx = change in concentration in a specific direction

D = diffusion coefficient.

The solution of equation (1) with appropriate boundary conditions gives the distribution of solute concentration, c, as a function of penetration, x, after time, t. The solution of equation (1) allows the diffusion coefficient to be calculated once the concentration distribution is known.

It has been experimentally determined that for small solute concentrations, values of the diffusion coefficients, D, may be related by a relation of the following form:

$$D = D_o \exp(-(E_a/kT)) \tag{2}$$

where D = diffusion coefficient

D_o = diffusion constant

E_a = activation energy

k = Boltzmann's constant

T = absolute temperature.

Equation (2) may be expressed in a logarithmic form as follows:

$$\ln(D) = \ln(D_o) - E_a/kT. \tag{3}$$

The coefficient of diffusion as outlined by Darken (16) is now recognized to be a function of concentration as well as other variables.

Diffusion constant values reported in the literature have a very wide range of values but 10^{+1} to 10^{-5} covers most materials. Ionic materials usually have diffusion constants of the 10^{-1} magnitude, and for self diffusion the values are usually close to one. Barrer (17) has tables of constants for self diffusion and for solute ions of several

salts. Barrer (18) relates the diffusion constant, D_o, to the entropy of activation and he notes that usually the larger the activation energy the larger the diffusion constant. Barrer states that a smaller diffusion constant, D_o, or a small change in entropy is associated with a small disturbance of the lattice when a solute atom passes into the activated state and likewise, a larger diffusion constant or change in entropy is associated with a larger disturbance of the lattice. Thus self-diffusion constants are usually larger than solute diffusion constants. Barrer also stresses the similar functional form of the constant in chemical kinetics used to help characterize slow or fast reactions and the association with the reaction degrees of freedom. According to Zenner (19) the diffusion constants associated with high-diffusion paths such as grain boundaries and plastic deformation are significantly smaller than those found in a single crystal or a non-deformed material. Zenner was able to relate the diffusion constant to the entropy of activation and the length of a diffusion step; a longer diffusion step and/or more avenues of movement would result in a larger diffusion constant value as well as a diffusion step with a larger lattice distortion.

Activation Energy

The activation energy, E_a, is schematically represented in Figure 5. The rate determining factor in the diffusion process is the activation energy.

Diffusion Mechanisms

Seitz (20) first suggested that there were only three basic diffusion mechanisms, and that all other proposed mechanisms were variations and/or combinations of these three basic mechanisms. The three basic

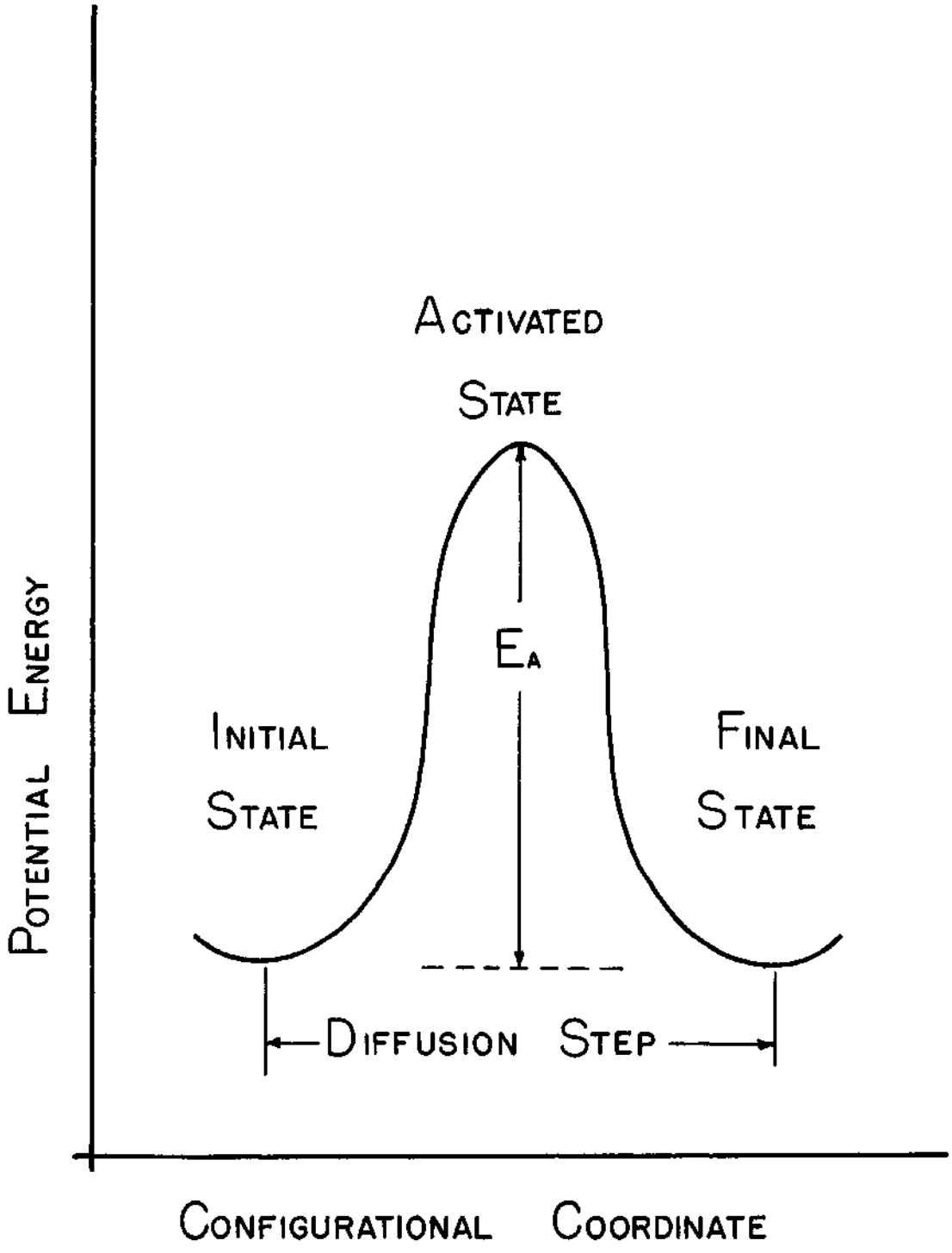

Figure 5. Activated State.

mechanisms Seitz listed were (a) an interstitial mechanism, (b) a vacancy mechanism, and (c) an atom-atom interchange. In an interstitial mechanism, a solute atom moves through the solvent by occupying successive interstitial regions in the solvent. Usually the solute atoms are small relative to the solvent atoms. Figure 6 is an example of the interstitial mechanism. Seitz described a case where if an interstitial atom could feasibly move a nearest-neighbor atom out of its position and take its place; the displaced atom may repeat the process so that the defect can move through the lattice. Seitz called this process an interstitialcy movement and classified the process as a variant of an interstitial mechanism. In a vacancy mechanism an atom next to a vacancy will move into the open region and a new vacancy is formed at the point where the moving atom departed. An example of the vacancy mechanism is shown in Figure 7. An atom-atom interchange is the relative movement (rotation) of two atoms about a midway point in which the atoms exchange places. Two atoms moving in this manner would require that near-neighbor atoms displace relatively large distances as is shown in Figure 8 by the two arrows. Seitz described a case where several atoms could move about a common axis in a ring manner as a modification of a direct interchange mechanism, illustrated by the three arrows in Figure 8.

Another case described by Seitz was when extra atom was found crowded into a plane of atoms. This mechanism was considered as a variant of the interstitial mechanism and was termed a crowdion.

Seitz listed the energies required for self-diffusion in metallic copper. These energies are given in Table 4. The energies for a vacancy and interstitial formation were found to be about equal, and the energy

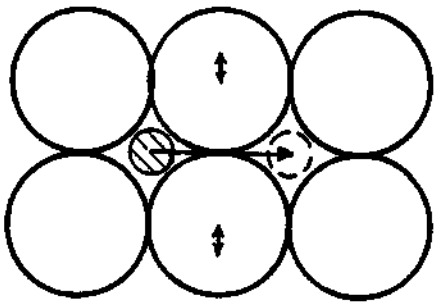

Figure 6. Interstitial Mechanism.
(Interstitial atom is shaded.)

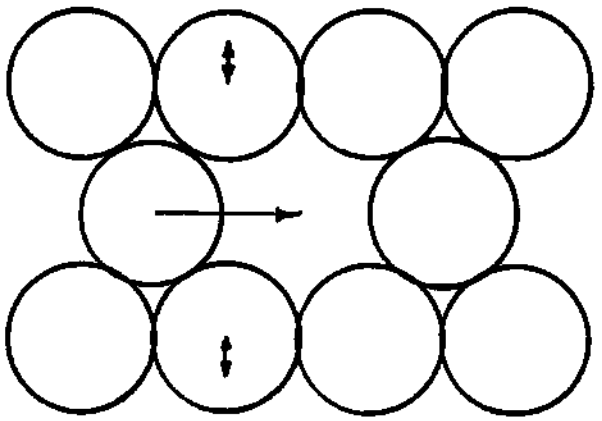

Figure 7. Vacancy Mechanism.

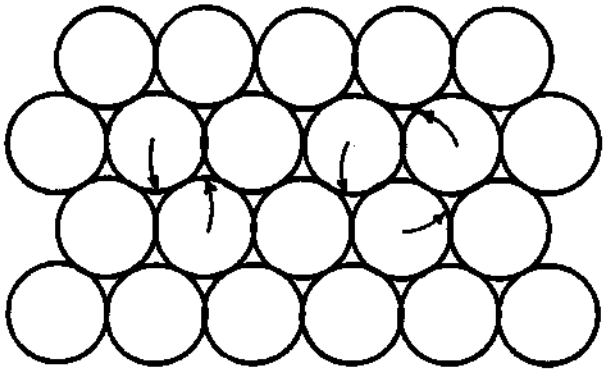

Figure 8. Atom-Atom Interchange.

required for an atom-atom interchange was found to be much larger than the other mechanisms as expected.

Table 4. Energies for Self-Diffusion in Metallic Copper

Energy	Electron Volts
Energy for direct interchange	11
Energy to take atom from surface to interstitial position	9.5
Activation Energy for migration of (approximately) interstitial atom	0.5
Energy to take atom from normal site to surface, thereby forming a vacancy	1.8
Activation energy for motion of vacancy (approximately)	1.0

Shewmon (21) has a more recent summary of diffusion mechanisms in which four basic mechanisms are defined; they are (a) ring, (b) interstitial, (c) vacancy, and (d) interstitialcy and crowdion mechanisms. A more detailed discussion of Shewmon's four mechanisms follows.

(a) Ring Mechanisms. A ring mechanism is a simple exchange of two nearest-neighbor atoms. In a closed packing arrangement, a two atom ring exchange would result in a large distortion of the lattice, thus requiring a great deal of energy. A three atom ring would have less distortion and require less energy. A similar argument follows for a four atom ring. The ring mechanism is not known to operate in any metal or alloy systems which is relatively close packed. To Shewmon, it seems plausible that this mechanism may be found to operate in open lattices. Shewmon

has apparently expanded the concept of an atom-atom interchange to include more than 2 atoms, and he has used the term ring to denote these movements.

(b and c) Interstitial and Vacancy Mechanisms. Shewmon's concepts of the interstitial and the vacancy mechanism are essentially the same as that of Seitz and no further discussion is necessary.

(d) Interstitialcy and Crowdion Mechanisms. In the case where solute atoms are approaching the size of the matrix atoms and these solute atoms are in interstitial positions, interstitial movement as discussed earlier is energetically prohibitive. However, if an interstitial atom shown in Figure 9 were to move or push its nearest neighbor atom into an interstitial position and then occupies the lattice site previously occupied by the displaced atom, the distortion of the matrix is small. This movement can occur with relative ease, and is called an interstitialcy mechanism.

For cases where interstitial atoms are the same size as the matrix ions, a configuration as shown in Figure 10 can exist, if the lattice is open enough to allow the doubling without undue distortion. Low energy movement can be accomplished by the pair rotating to extend in another direction, or one of the interstitial atoms can displace one of the nearest neighbor atoms so that the original structure site forms another doubly occupied site.

Still another interstitial configuration is called the crowdion. It has the extra atom placed in a close-packed direction, thus displacing several atoms from their equilibrium positions as shown in Figure 11. Its distortion is spread out along a line, and it can glide in only one

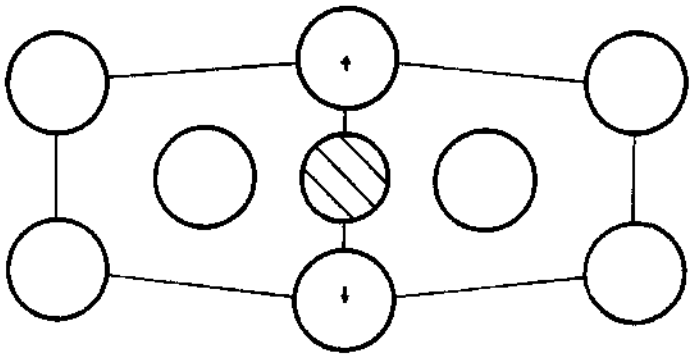

(interstitial atom is shaded)

Figure 9. Interstitialcy Mechanism With Ion Sizes About Equal.

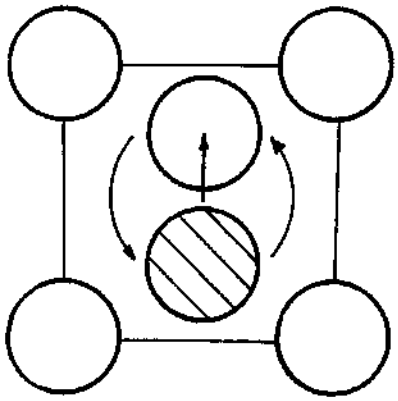

(interstitial atom is shaded)

Figure 10. Interstitialcy Mechanism With Ion Sizes Equal.

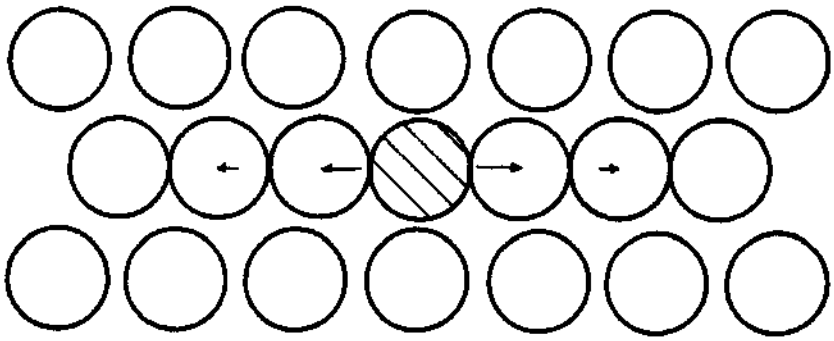

(interstitial atom is shaded)

Figure 11. Crowdion Mechanism.

direction; the energy required for movement is quite small. Large atom interstitials are not found in close packed structures unless high energy working has occurred, i.e., cold working and high energy particle bombardment.

Shewmon apparently classifies the two special cases defined by Seitz, interstitialcy and crowdion processes, as mechanisms rather than a variant of the interstitial and atom-atom mechanism.

Vapor Diffusion Couples

Each of the three main boundary conditions for which solutions to equation (1) are used in diffusion experiments are illustrated in Figure 12. There are advantages and disadvantages to each set of conditions. Wuensch and Vasilos(21) give an adequate discussion of the advantages and flaws of each method. Wuensch and Vasilos (22) used a vapor-deposition diffusion couple because of the vapor pressure of the solute and because of the amount of material needed for adequate solute penetration. The solution to equation (1) was:

$$C(x,t) = C_o(1 - \mathrm{erf}(X(4Dt)^{-\frac{1}{2}}) \qquad (4)$$

where $C(x,t)$ = concentration at x distance from the surface at time t

erf = Gaussian error function

D = diffusion coefficient.

This technique gave excellent results even when there was a buildup of the deposited material on the matrix surface. Another unusual aspect of the experiment was that an electron microprobe was used to analyze

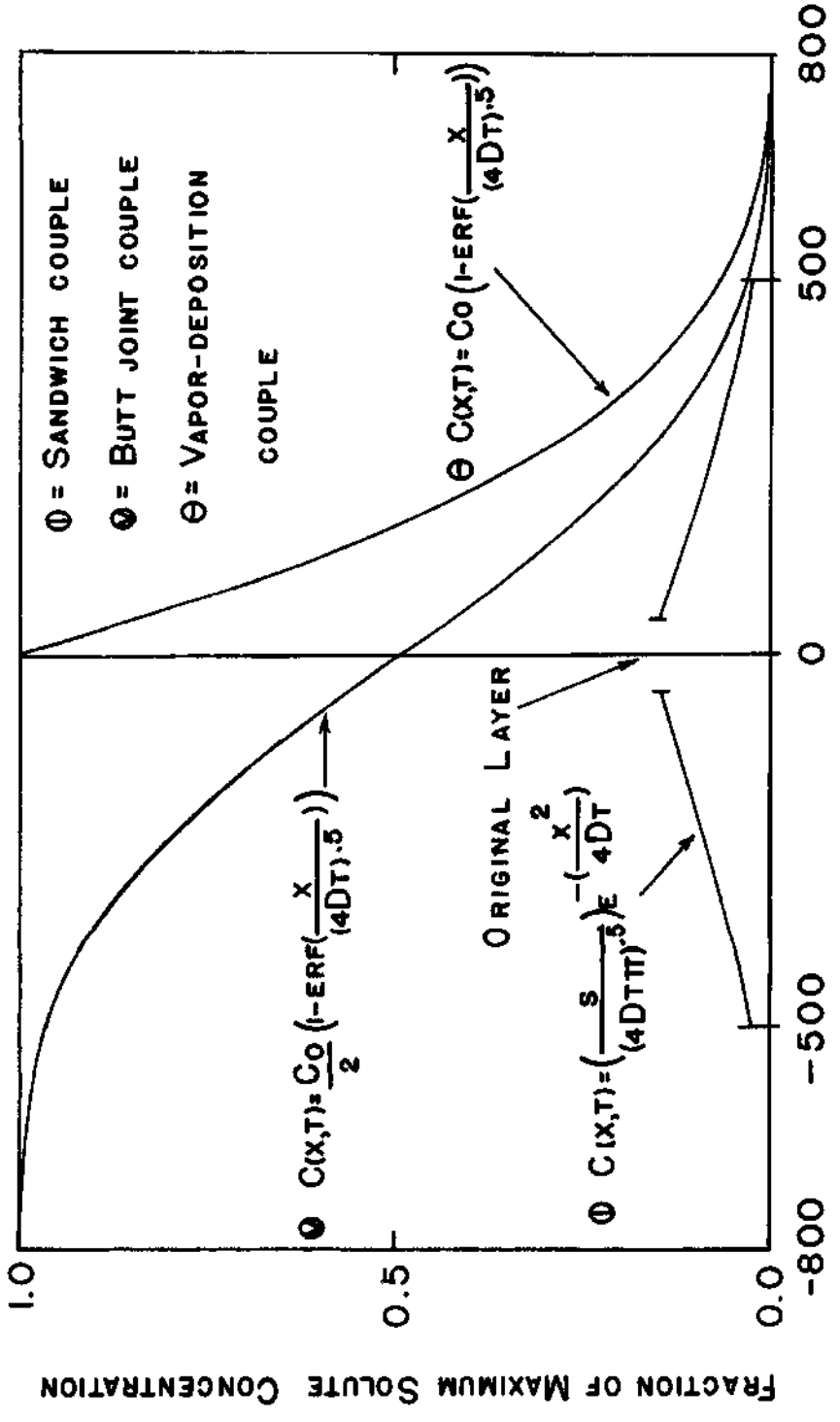

Figure 12. Solute Distribution for the Three Main Boundary Conditions.

for the solute concentration. The results using this instrument compared very well with tracer methods of analysis.

CHAPTER III

INSTRUMENTATION AND EQUIPMENT

Equipment

Molten NaCl Holder

A refractory box was constructed of a castable refractory mix as shown in Figure 13. Harbson-Walker Harcast refractory was used to construct the container. It had one inch thick walls and an inter-chamber one inch wide by three and three quarter inches deep. The chamber was divided into two parts, the charging end and the treatment end. A cover made of similar material was used over both the charging and treatment end. The treatment end cover had four holes about one quarter of an inch in diameter. The NaCl vapor traveled up through these holes and around the samples which were placed over the holes.

Kilns

Gas Fired Kiln. For tests conducted at 1100°C and higher, an Ibsen model B-L-35 High Temperature Box Furnace was used. The kiln used natural gas and a blower. The gas and air were premixed before they reached the burner. A two-position valve was used to control the amount of air-gas mixture delivered to the burners. Through a recorder and an off-on controller the temperature could be brought to a desired value and held there by regulating the air-gas valve.

Electric Kiln. For tests conducted at 900°C and 1000°C an electric kiln was used. The kiln was a muffle electric type. In a

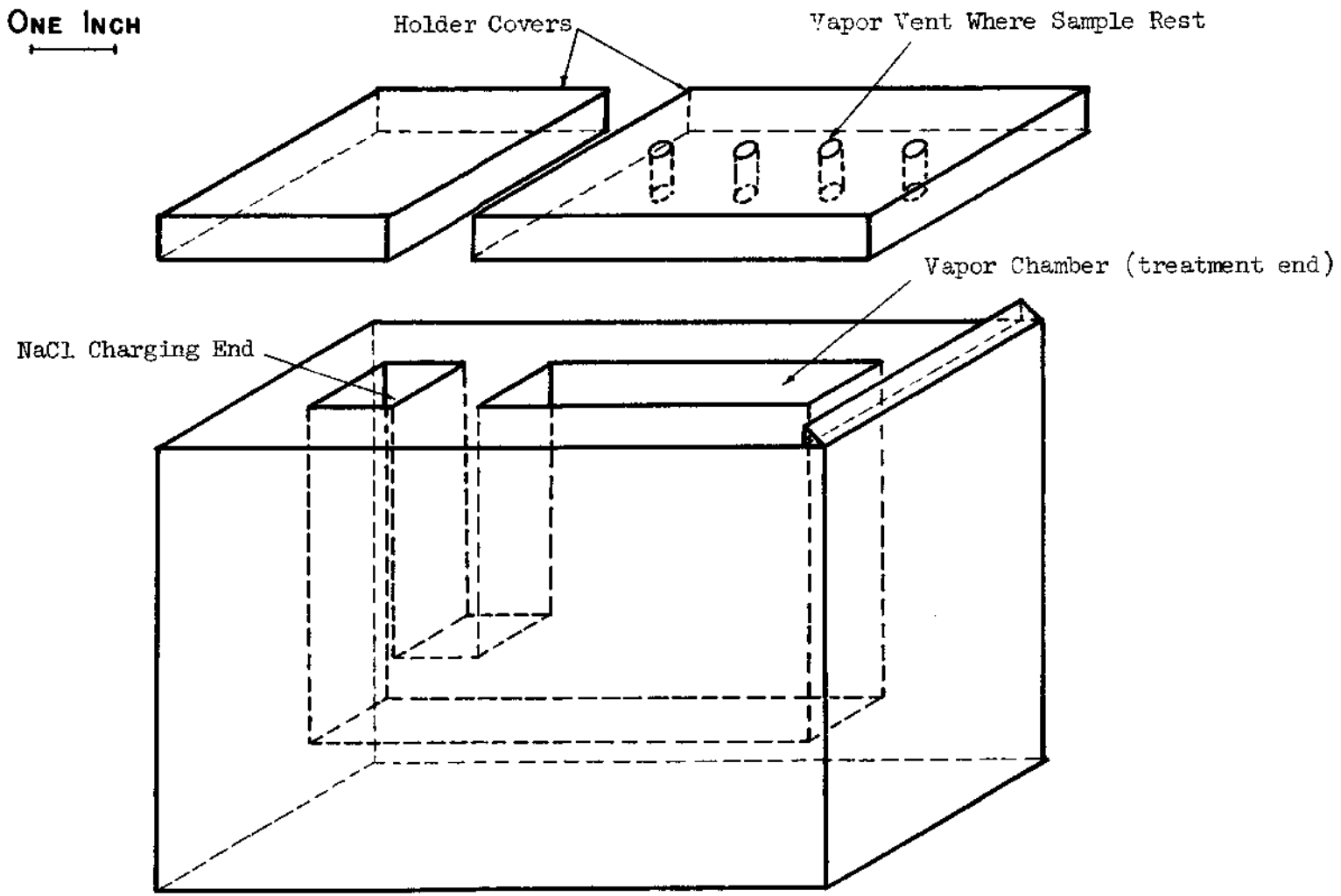

Figure 13. Molten NaCl Holder with Covers.

section drawing of the kiln, Figure 14, it can be seen that the design was simple and straightforward. A Wheelco controller driving a 5.0 kilowatt saturable core reactor was used to power the kiln.

Polishing Apparatus

A sleigh type sample positioner was used to polish a perpendicular face on crystal samples. In Figure 15, the sleigh slid over the working surface, while the sample was held with the fingers against the sleigh and on top of a strip of polishing paper. Paper with an adhesive backing and of 320 and 600 grit was positioned parallel along the working surface. The sleigh was shaped so that a sample could be polished 0°, 90°, or 45° with respect to the long axis of the working surface. The supports were aluminum, the sleigh runners were steel, and the remaining portions were brass.

Instruments

X-ray Diffraction

A Norelco diffractometer was used with a copper source for x-rays. A nickel filter, a receiving slit of 0.003 inches width, and a one degree angular aperture were used with the diffractometer. The detector used was a sealed proportional counter. The source was operated at 40 kilovolts and 24 milliamps. The pulse height analyzer was set such that 90 per cent of the apparent radiation being diffracted from a silicon sample would be registered.

Electron Microprobe

An electron microprobe was used to analyze the samples for the different elements. The instrument used was an Acton electron micro-

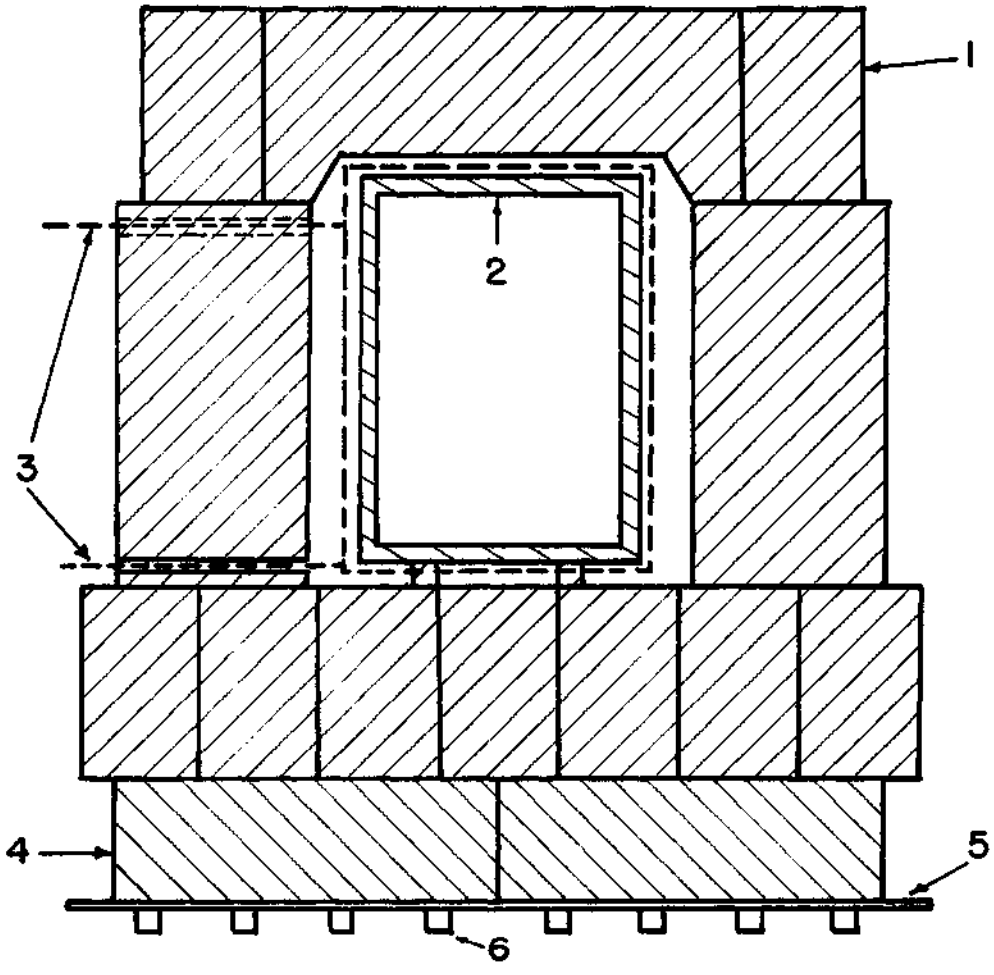

1. High Temperature Insulating Firebrick
2. Alumina Muffle 5.75x8x14 inchs
3. Electric Heating Elements
4. Low Temperature Insulating Firebrick
5. Aluminum Sheet 3/4 inch Thick
6. Supports

Figure 14. Electric Muffle Kiln.

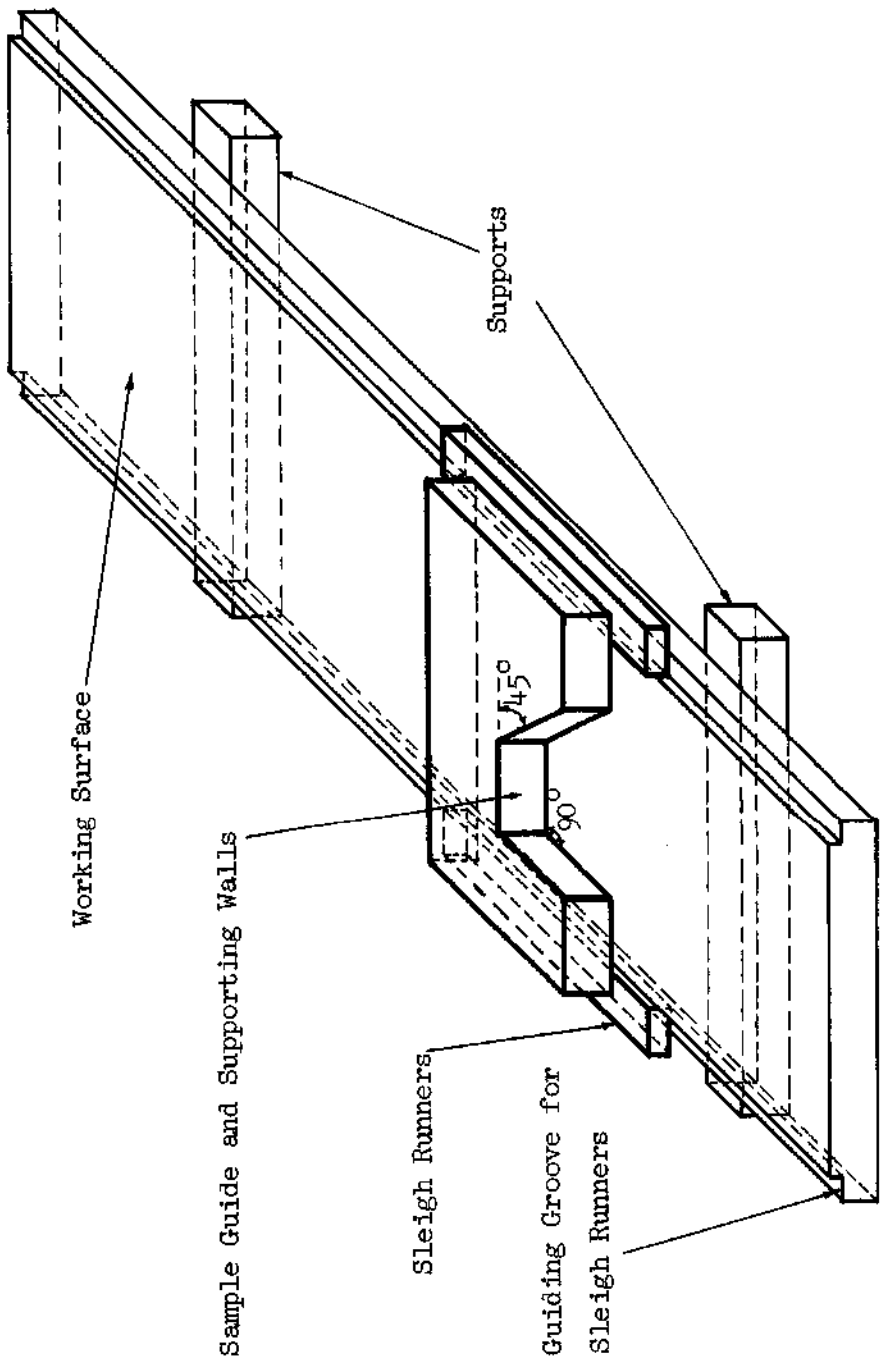

Figure 15. Polishing Apparatus.

probe model MS-64 made by Acton Laboratories of Acton, Massachusetts. The basic operating principles of an electron probe can be illustrated with a schematic diatram such as Figure 16. Electrons were accelerated down a column and focused into a narrow beam. For the Acton probe, a voltage of 20,000 volts DC was used to accelerate the electrons. The manufacturer claims that the electron beam is focused to a diameter less than 1.0 micron and more than 0.1 micron; a diameter of 0.6 to 0.8 microns was considered to be the actual beam diameter by the operator.

The electrons striking the sample had enough energy to knock electrons out of the orbits of the sample atoms. When the electrons returned to their normal positions, x-rays were emitted. The energy or wave lengths of these x-rays were unique for each of the elements. By examining the emitted x-rays, a determination of what elements and the amounts present was made. The x-rays were sampled at a specific angle from sample surface; for the Acton probe, this angle was 18°. The sample x-rays were allowed to strike an analyzing crystal which separated the different x-rays according to their wave length. A mica crystal was used as the analyzing crystal in an Acton probe. Once the x-rays were separated, a detector was used to determine which energy levels of x-rays were present. A gas flow proportional counter was used to determine the presence of the x-rays.

The electron gun, sample, analyzing crystal, and detector were in an evacuated chamber at about 20 microns of Hg pressure. The vacuum helped reduce intensity losses to a minimum.

Because electrons from the electron gun would build up on the

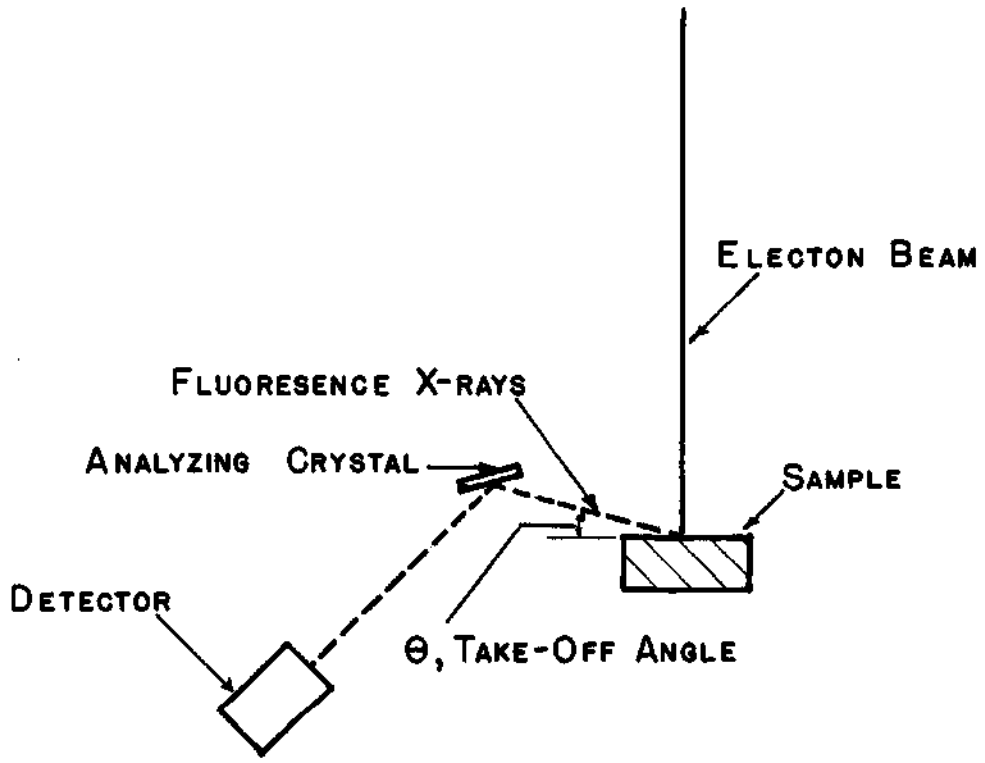

Figure 16. Schematic of an Electron Microprobe.

sample and give it a negative charge and cause the electron beam to become unstable, a thin layer of carbon, 100 angstroms thick, was deposited on the sample surface to provide a conducting path for the electrons. The electron flow, current, from the sample was carefully regulated; it was held to 100 nanoamps ± less than 0.1 per cent by a feed back regulator.

Some of the x-rays that were emitted by the elements of the sample caused other elements of lower atomic number to emit x-rays, secondary radiation. The secondary radiation was found to be emitted in an area of about 5 microns in radius around the electron beam striking point. Two micrometers with one having a motorized drive was used to move the sample. The electron beam was focused manually on the sample surface by the operator.

Polarizing Microscope

A standard mineralogical polarizing microscope and a standard set of oils were used to determine index of refraction, birefringence, and optic sign of the mineral specimen.

Mass Spectrometer

The mass spectrometer used to carry out spectrographic analysis was a Bendix Time of Flight Mass Spectrometer with a Knudsen cell sample inlet system. The spectrometer ionizes emitted vapor species from a sample and accelerates the ions down a path with a large electric potential. The time it takes for an ion to travel the path distance is a function of the ion's mass and charge.

CHAPTER IV

EXPERIMENTAL PROCEDURE

Preparation of Samples

Preparation of Powdered Samples

Several crystals were selected to be gound into a powder. The crystals had excellent hexagonal morphology and were completely clear to the unaided eye. The grinding was accomplished with a mortar and pestle and then screened to pass a 325 mesh screen.

Preparation of Single Crystal Wafers

Crystals, which were of excellent morphology, clear to the unaided eye, and were large enough so that a three-eights inch or larger diameter wafer could be obtained from them when sectioned, were selected for use in the experiments. The crystals may have had some small cracks which could not be observed. The selected crystals were mounted on a wooden base with jewelers' wax. The crystals were covered with the wax so that the cut slices would not be damaged by the saw blade. By using the morphology, the c-axis was located and the crystals were positioned on the board so that the saw would cut the crystal either parallel or perpendicular to the c-axis.

A diamond saw with water coolent was used to cut the crystals. Wafers were cut about 75 thousandths of an inch thick. After slicing, the wax was removed with a knife. One of the large area sides of the wafer was polished with a 600 grit paper and washed with Ethanol. The crystals were then stored until needed.

A part of each crystal was saved to be used to determine the amount of chlorine occurring in a wafer naturally. However, a crystal piece for four wafers were not saved and chlorine analysis could not be made. The crystal pieces were mounted in a plastic mounting material, and polished using a 600 grit paper.

Treatment of Samples

Treatment of Powdered Samples

The powder sample was split, and one part was not subjected to any treatment. The second part was heated to 1200°Centrigrade for one hour and allowed to cool. The fired powder was lightly ground and passed through a 325 mesh screen to break lumps formed due to a slight amount of sintering that took place. The fired and natural samples were stored in air tight bottles.

Treatment of Single Crystal Wafers

Density Measurements. Several of the wafers were used to determine the density of the material used. The wafers were first weighed in air and then suspended in distilled water.

Diffusion Test. For each test condition, four crystals were selected, two cut parallel and two cut perpendicular to the c-axis. Once selected, the crystals were assigned an identifying number.

The samples were then placed over the holes in the molten NaCl holder cover with the polished face down against the holder. The holder loaded with NaCl and crystals was loaded into the kiln used for the test. In Appendix A the test conditions are listed and the kiln used for the test is indicated. For the higher temperature runs, molten rods of NaCl

about one half of an inch in diameter were used to recharge the NaCl container. At lower temperatures, the rate of evaporation of the NaCl was such that recharging was unnecessary or infrequent. The test conducted at 1200°Centigrade, was slightly different. In these tests, Al_2O_3 less than 44 microns in diameter, was mixed with NaCl to slow down its evaporation. No special order of firing was established or carried out.

Data Collection From Samples

Powder Samples

With each of the powders, an x-ray diffraction pattern was prepared. The peak maximum points were determined and the corresponding angular value converted to interplaner distance. Interplaner spacings were associated with a particular plane by assigning to the spacing an (h,k,l) Miller indices value. A standard card, American Society for Testing Materials card number 9-432, for hydroxyapatite was used to assign (h,k,l) values.

A small portion of the heated and natural sample was used to determine the index of refraction and birefringence of the samples. The index of refraction of the powders was compared with those of standard oils until a match was obtained. A match was made when the ordinary and the extraordinary rays were being viewed. Oils were mixed if the sample indices were between two standard oils.

A small portion of the unheated sample was subjected to a mass spectrographic analysis. The sample was heated to about 1430°C in 15 to 20 minutes in a vacuum, and the vapor species being emitted from the sample were detected; the masses of these species and the relative amounts

present were recorded. Apparent appearance potentials for the masses were not determined. The peak intensity or relative amount for each mass detected was recorded at each of the increasing temperature steps.

Single Crystal Wafers

Only the weights in air and in water were recorded for the wafers in density measurements.

Once the wafers were removed from the kilns, the area exposed to the direct NaCl stream was identified and marked with a graphite coating. Then using a knife edge and a heavy object to strike the blade, the crystal was broken across the marked area. A suitable piece was selected which included some of the marked area, and a surface was ground parallel to the direction of diffusion. The polishing apparatus, Figure 11, was used to form the surface. The last polishing step was such that the strokes were parallel to the flat face of the wafer. The sample was then cleaned with Ethanol.

The wafer was ready for a probe scan after cleaning. A Cl scan was made of the crystal. An area where there was the least amount of distortion of the edge was probed. If any unusual features appeared on the trace, another trace in another area was made. Scans were made for sodium in selected crystals. At least one scan for sodium was made for each type of crystal cut in a time-temperature treatment combination.

Counts of the amount of chlorine radiation being emitted from a sample were made in areas of the sample not penetrated by the chlorine. Counts of a synthetic chlorapatite were made and counts of the background were made to enable the analysis of the sample for chlorine to be made.

Natural Chlorine Content. The amount of chlorine radiation emitted

in a given length of time (number of counts) was determined for the crystal pieces using the electron probe. The number of counts for synthetic chlorapatite and the background noise was recorded.

Data Calculations

Powder Sample Calculations

Two planes were used to calculate the a-axis length. If the interplaner distance for the (100) plane is divided by the cosine of 30 degrees the resultant value is the a-axis length. The second plane used was the (110) plane. If the (110) distance is doubled the resultant is the a-axis length. The c-axis length was calculated using the (002) and (004) interplaner distance. If the (002) plane distance is doubled, and the (004) distance multiplied by four, the resultant is the c-axis length.

The birefringence was determined by subtracting the ordinary ray's index of refraction from that of the extraordinary.

Single Crystal Wafer Calculations

The density of the wafers was found by dividing the difference in the weight in air and in water by the weight in air.

The chlorine probe scans were marked off at every micron unit and a listing was made of the count rate and distance from the edge. The listing continued until the count rate values leveled off. On this list the count rate values were adjusted to indicate the intensity above the leveled value, I_o, and they were entered in another column. Another column was prepared where the adjusted intensity, C, was divided by C_o, the difference between the maximum intensity value and the level intensity value. A computer program, Appendix B, was used to find the least square fit of

equation (4) to the data. In this process the value B was found such that:

$$B = 1/(2(Dt)^{\frac{1}{2}}) \tag{5}$$

where: B = fitted least square constant

D = diffusion coefficient

t = time.

The activation energy, E_a, and the diffusion constant, D_o, were found by fitting a straight line to the plot of ln(D) verse 1/T, where T = the absolute temperature. An example of this procedure is given in Appendix C.

The per cent chlorine in the apatite was found by plotting the background average count per 20 seconds as 0 per cent chlorine and the synthetic chlorapatite average count per 20 seconds as 6.82 per cent chlorine on a linearly scaled graph and drawing a straight line between these two points. The average count per 20 seconds for each unknown point was determined and, by finding the intersection of this count with the constructed line, the per cent chlorine was read from the graph. Figure 17 is a schematic diagram of the per cent chlorine determination. The samples were analyzed in groups of 3 to 6, and a background and synthetic chlorapatite count was made when each group was analyzed.

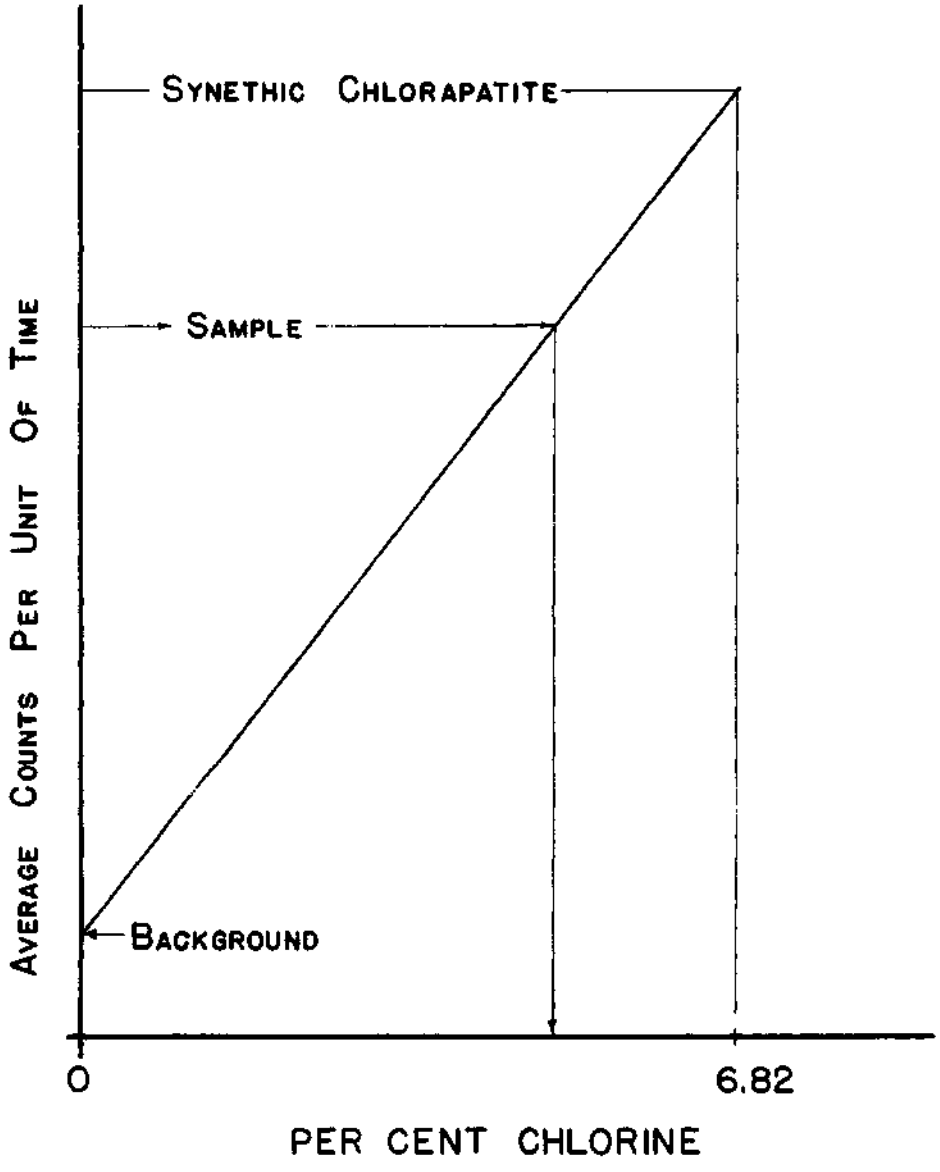

Figure 17. Schematic of Per Cent Chlorine Determination.

CHAPTER V

DISCUSSION OF RESULTS

A. Identification of the Durango, Mexico Apatite Used

Density

The density of the apatite was found to be 3.22 ± .01 grams per cubic dentimeter. The density reported is the average density of those in Table D-1, Appendix D. The density is in agreement with the densities of 3.2 grams per cubic centimeter for a fluorapatite as reported by Larsen and Berman (9) and 3.218 grams per cubic centimeter, as found by Bhimasenacher, (7). The Durango Apatite density was significantly higher than the densities, Table D-2, Appendix D, of a hydroxyapatite and a chlorapatite and appears to be essentially that of a fluorapatite.

Index of Refraction

In Table 5 the optical properties are listed. The accuracy of the determination was limited as it was difficult to find a particle with its optic axis perpendicular or near perpendicular to the microscope stage. In addition to obtain oils with indices of the values derived, mixing of two oils was necessary. Larsen and Berman (18) listed the indices for a fluorapatite as 1.630 and 1.633 for the extraordinary and ordinary rays respectively. Their values are close to the experimentally determined indices, and the birefringence is within experimental error, the same. The indices were about two-thousandths higher for the sample than those reported by Larsen and Berman. The indices were

significantly lower than the 1.65 to 1.67 range for hydroxy and chlorapatite as reported by Elliott and Young (12). Indices of refraction found for the Durango Apatite are very close to those of a fluorapatite and apparently, the Durango, Mexico Apatite used was a fluorapatite with possibly some small impurity.

Table 5. Optical Properties of Durango, Mexico Fluorapatite

A.	Indices of Refraction
	N_e = 1.633 ± .001
	N_o = 1.635 ± .001
B.	Birefringence - .002 ± .002
C.	Sign - Uniaxial, negative
D.	Strain present in crystals

Chlorine Content

The average chlorine concentration, Table D-3 Appendix D, in the samples used was 0.53 ± .04 per cent. Other investigators, Table 2, did not report chlorine concentration and a comparison was not possible. A pure chlorapatite would contain about 6.82 per cent chlorine by weight. The samples contained less than one tenth of the amount of chlorine a pure chlorapatite would contain. It appears that the samples used in the experiment had, on the average, about eight unit cells of chlorapatite per hundred fluorapatite unit cells.

Lattice Parameters

The lattice parameters found for the Durango Apatite are given

in Table 6. These values were calculated from the diffraction spectra given in Table D-4, Appendix D. The discrepancy between the two independent calculations for the axis lengths appear to be within the error range of the equipment. Small deviations, one-hundredths of a degree, in fixing the 2θ value of (100) plane will generate as much as 0.01 angstroms error in the a-axis length. Three-hundreths of a degree deviation in the (110) plane peak location will generate a 0.01 angstrom error. An error of one-hundreths of a degree in the (002) peak location will generate a 0.003 angstrom error while an one-hundredth of a degree error in the (004) peak location will generate a 0.001 angstrom error. The error associated with reading the diffraction pattern was estimated at no more than plus or minus two-hundredths of a degree for all of the peaks. Machine errors were the alignment of the diffractometer with the strip chart recorder and alignment of the diffractometer itself. The machine error was considered to be plus or minus one-hundredth of a degree. These errors will most likely cancel themselves out; however, an overall error of one and one half hundredths of a degree was used as an estimate of the total error for the peaks.

Table 6. Lattice Parameters of Durango, Mexico Fluorapatite

a-axis (angstrom)	Reference Plane for Calculation	c-axis (angstrom)	Reference Plane for Calculation
9.410 ± .015	100	6.876 ± .005	002
9.404 ± .005	110	6.884 ± .002	004

The a-axis length was found to be slightly longer than that found by Trautz (5) and Carlstrom (8) in Table 3. The c-axis length was found to be about the same as the values in Table 3. The same can be said for the fluorapatite parameters reported in Table 1. The a-axis length is not as long as that in Table 1 for hydroxyapatite and chlorapatite. The c-axis values of the hydroxyapatite and fluorapatite are about the same, and the c-axis value in Table 6 could be classed as belonging to either of the two, but not that of chlorapatite.

A positive identification of the material from a comparison of lattice parameters was not possible, however, a fluorapatite identification could not be rejected. The Durango apatite a-axis lengths in Table 3 are somewhat larger than values for synthetic fluorapatite, indicating there may be a range of a-axis lengths for the Durango apatite. Two possible reasons for the spread in the values may be strain and a variable amount of substitution of OH^- and/or Cl^- for F^- in the crystals. The substitution of OH^- can not be ruled out because the chemical analysis in Table 2 are incomplete, but there is little to suggest that significant amounts of OH^- are present in the material. Chlorine was found, Table D-2, Appendix D, to be an impurity in the apatite. On the other hand, some strain, Table 5, was found in the material. Strain could have been introduced in the grinding of the samples.

Mineral Identifcation

The density, chemical, optical, and lattice parameter measurements strongly indicate that the material was a fluorapatite rather than a chlorapatite or a hydroxyapatite. The optical and density measurements best indicated that the material was a fluorapatite. Optical,

chemical, and lattice parameter measurements indicated that the crystals were strained, and that they contained some chlorine impurity.

B. Changes in the Durango, Mexico Fluorapatite Properties on Heating to 1200°C

Index of Refraction Changes

The optical properties of the heated specimen are listed in Table D-5, Appendix D. The indice for the extraordinary ray did not change, but the ordinary ray indice increased to 1.637 ± .001. The birefringence increased from 0.002 ± .002 to 0.004 ± .002. No other changes in optical properties occurred during the thermal cycle. In all probability, the apparent increase in the ordinary indice and birefringence is insignificant because of the errors associated with the indice measurements.

Diffraction Spectral Changes

The diffraction spectra of the heated apatite is given in Table D-6, Appendix D. Table 7 is a comparison of the natural and heated apatite diffraction spectra. Intensity changes of plus or minus ten per cent or less could possibly be due to machine and particle packing differences. Intensity differences of ten or more per cent are apparent shifts of peak intensity relative to the (211) peak intensity. The (002) and (112) peaks increased significantly in intensity relative to the (211) peak intensity, and the (300), (222), and (213) decreased in intensity significantly. The significance of the intensity changes was not readily apparent.

Spacing shifts, Table 7, for the (100) plane and other related planes, i.e., (110), (101), etc., were the largest and changes associated with the c-axis were small by comparison. The lattice appears to have

become more compact, particularly in directions perpendicular to the c-axis on heating. The shifting of the atoms on heating may have been due to the emission of impurities such as chlorine and possibly carbon, and/or the release of strain in the lattice.

Table 7. Change in Durango, Mexico Fluorapatite Diffraction Spectra on Heating to 1200°C

Plane Miller Indices	Change in Relative Intensity	Change in Plane Spacing in Angstroms	Plane Miller Indices	Change in Relative Intensity	Change in Plane Spacing in Angstroms
100	-1*	-0.03**	310	-1	-0.005
101	-1	-0.020	221	-1	-0.006
110	-1	-0.018	311	+1	-0.004
200	+1	-0.012	113	-1	-0.001
111	-1	-0.009	203	-1	-0.002
201	-3	-0.003	222	-14	-0.003
002	+16	-0.003	312	+2	-0.003
102	+2	-0.006	320	+4	-0.003
210	+4	-0.006	213	-26	-0.002
211	0	-0.006	321	-3	-0.003
112	+15	-0.005	410	0	-0.002
300	-25	-0.006	402,303	+4	-0.003
202	-3	-0.002	004,411	+2	-0.001
301	-3	-0.006	322,223	+1	-0.002
212	+1	-0.004	313	+2	-0.001
			501,204	0	

*Natural Minus Heated Intensities

**Natural Minus Heated Spacings

Lattice Parameter Changes

Table 8 is a list of the a and c-axis length changes on heating. The two values calculated for each axis appear to be within the error limits as previously described. The average change for the a-axis was a 0.033 angstrom decrease, and for the c-axis the change was, on the average, a 0.005 angstrom decrease or about a sixth less than the a-axis decrease.

Table 8. Durango, Mexico Fluorapatite Lattice Parameter Changes on Heating to 1200°C

	a-axis length (angstroms)	c-axis length (angstroms)
Before Heating	9.41*	6.876***
	9.404**	6.884****
After Heating	9.38*	6.870***
	9.368**	6.880****
Change	-0.03*	-0.006***
	-0.036**	-0.004****

*Calculated using (100) plane spacing
**Calculated using (110) plane spacing
***Calculated using (002) plane spacing
****Calculated using (004) plane spacing

These changes suggest that the lattice apparently became more densely packed in directions perpendicular to the c-axis and only slightly more tightly packed in the direction parallel to the c-axis. The smaller lattice parameters agree well with the fluorapatite parameters in Table 1 and Table 3.

Possible causes for the apparent axis shorting are the release of strain and/or the emission of impurities. If chlorine impurities occupied anion positions in the fluorapatite lattice, an expanded a-axis, Figure 3, could have been the result. Distortion of the lattice could have occurred around the impurities, thereby inducing some strain in the lattice. Elliott and Young (12) report chlorine can be removed from an apatite at the temperatures of the experiment, 900° to 1300°C. If chlorine was removed

the strain and distortion could have been relieved, and the a-axis possibly shortened. The removal of the chlorine may not have accounted for all of the reduction in the a-axis. Other possible impurities such as carbon may have been responsible for some of the distortion and expansion of the a-axis, which on heating would have been removed. Any strain induced in the lattice when crystals were ground for x-ray studies could have been released on heating. The most reasonable cause for the a-axis length decrease seemed to be a combination of strain release and impurity emission. The heating of the apatite appeared to remove imperfections in the crystals by reducing the amount of impurities and by relieving strain.

Possible Effects of Structure Changes During Heating on Diffusion

The rearrangement on heating of the apatite structure, an apparent shortening of the a-axis, could have influenced the diffusion rates of anions in directions perpendicular to the c-axis. The c-axis length had only a small reduction which likely had little or no effect on the diffusion rates of anions parallel to the c-axis. The shortening of the a-axis and the release of the strain could have accelerated the anion diffusion rates. On the other hand, if the release of strain and the reduction of the a-axis was completed before a significant amount of diffusion had taken place, then the results could have been freer from the effects of possible imperfections in the crystals.

C. Mass Spectrographic Analysis of the Durango, Mexico Fluorapatite

Tables of the mass intensities for temperatures up to 1430°C

are in Appendix E. Of special interest were the equivalent masses of calcium, phospherous, oxygen, fluorine, chlorine, and carbon dioxide, since these elements are the components of fluorapatite or known impurities.

Masses 40, 31, 19, and 16

The masses of Ca, P, F, and O are 40, 31, 19, and 16 respectively. The measured intensities of masses 40, 31, and 19 were less than 0.7 units. Background was approximately 0.1 units and 0.2 unit was considered a definite peak. At these levels of intensities, 0.7 units or less, small concentrations of ions with masses of 40, 31, and 19 may be elemental ions or ionized molecules, both organic and inorganic such as CH_4, mass 16, and O_2^{2-}, apparent mass 16. Probably there were Ca, P, and F ions released from the sample but the low intensities for the masses, 40, 31, and 19, indicates that the amount lost was insignificant. The higher mass 16 intensities, maximum of 7.0, can probably be assigned to oxygen, but the major source of the ion may not be the sample material. There were many likely sources of oxygen in the system, such as the residual atmosphere, leaks, adsorbed oxygen on the surface of the sample and components of the sample inlet system, "out gassing" of contaminates, and the dissociation of water or other oxygen containing compounds. The major source of the mass 16 ion could not be determined, however, the amount of oxygen emitted from the sample was likely small since the amount of oxygen given off from the dissassociation of water appeared to be very large; an examination of the mass 17 and 18 intensities indicated that there were apparently large quantities of OH and H_2O present.

Masses 35, 37, and 44

The mass weights for the chlorine isotopes are 35 and 37 in a 3 to 1 ratio respectively and the mass weight for carbon dioxide is 44. Some of these masses should be found in the mass spectra since the sample was found to contain about 0.5 per cent chlorine by weight and may have contained some carbon dioxide, Table 2. The intensities of masses 35 and 37 were low, less than 0.4, and appeared only at higher temperatures. The low intensities suggested that the amount of mass 35 and 37 present was insignificant, and the intensities did not follow the 3 to 1 ratio for the chlorine isotopes. Probably there were some Cl ions present, however, the amount present appeared to be insignificant.

The presence of mass 44 in apparently significant amounts; maximum intensity of 13.0, indicated that the carbon dioxide ion was present, however there were many possible sources of the carbon dioxide ion. Some of the possible sources of CO_2 were the sample, "out gassing" of contaminates, adsorbed molecules of the surfaces, and decomposition of vacuum seals. Elliott and Young (12) found that carbon dioxide was released from an apatite at or about 800°C, under normal atmospheric conditions, and at a fast heating rate the emission temperature could appear to be higher than equilibrium conditions; this may help explain the apparent higher emission temperatures. On the other hand a lower emission temperature would be expected in a vacuum than at standard atmospheric conditions. Near 800°C another method of heating the sample was employed which may have heated areas other than the sample holder and sample, thus activating new sources of CO_2. The sample probably did release some CO_2 and it appears that it was released above 1000°C.

Significant Mass Intensities

Apparent significant mass intensities, more than 0.7, found were those of the masses 2, 17, 18, 27, 28, 29, 32, 33, 34, 36, 41, 43, 55, 64, and 78. Masses 2, 17, 18, and 32 appeared to be H_2, OH, H_2O, and O_2 respectively. Masses 36, 55, and 78 may have been the ions HCl, $CaCl_2$ doubly ionized, and CaF_2 respectively. Mass 28 could have been the ions N_2, CO, or CaO doubly ionized or a combination of the ions. Masses 27, 29, 33, 34, 41, 43, and 64 could not be matched with readily suggested inorganic molecules.

If masses 36 and 55 were considered to be HCl ions and $CaCl_2$ doubly ionized ions respectively, then the loss of chlorine could be considered significant, and the chlorine loss would agree in principle with the loss in chlorine content as indicated in Table 8. The most likely source of any chlorine appeared to be the sample. If mass 78 is considered to be the CaF_2 ion, then a small amount of fluorine may have been released from the sample. The most likely source of any fluorine was the sample.

Insignificant Mass Intensities

Apparent insignificant mass intensities, less than 0.7, found were those of the masses 12, 14, 15, 20, 26, 30, 38, 39, 42, 46, 48, 56, 57, 58, 60, 62, and 70. Masses 12 and 56 appeared to be C and CaO respectively. Masses 15, 38, 39, 46, and 57 may have been the ions CH_3, HCl, CaF_2 doubly ionized, NO_2, and $CaCl_2$ doubly ionized respectively. Mass 20 may have been the ions HF or Ca doubly ionized, mass 30 may have been the ions NO or C_2H_6, and mass 62 may have been the ions P_2 or H_2CO_3. Masses 26, 42, 48, 58, 60, and 70 could not be matched with readily suggested

inorganic molecules.

Possible Influence of the Thermal Cycle on the Diffusion of Anions

The mass spectrometer analysis indicated that the Durango, Mexico Fluorapatite lost some chlorine, carbon dioxide, and to a lesser extent fluorine on heating to 1430°C. A reduction in the chlorine and carbon dioxide content could have increased the orderness of the fluorapatite, and, on the other hand, a possible loss of fluorine could have created crystalline defects such as vacancies which could aid the diffusion of anions. The analysis indicated that significant amounts of Ca, P, or O, (masses 40, 31, and 16) were not released from the sample, in which case the basic apatite structure could be considered to be stable and may or may not have any effect on the diffusion of anions.

D. The Amount of Chlorine Released on Heating

The heated samples which were exposed to a NaCl vapor were analyzed for chlorine in an area away from any apparent influx of chlorine; the chlorine concentrations are listed in Table 9. Most of the samples had an apparent decrease in the chlorine concentration, sample 132 was an exception with an increase of chlorine content. The general decrease in chlorine content confirms the indications of x-ray and optical measurements that some chlorine was removed on heating. The NaCl vapor pressure may have inhibited the complete release of chlorine, however there appeared to be a significant decrease in the original chlorine concentration. The remaining chlorine in the apatite may possibly have affected the anion diffusion rates.

Table 9. Sample Chlorine Concentration Before and After Heating

Test Conditions Temperature Time	Sample Number	Principle Direction of Diffusion From c-axis	Starting Concentration (%)	Treatment Residual Concentration (%)	Change in Concentration (%)
900°C	116	parallel	0.57	0.25	0.22
64 hours	117	parallel	0.47	0.24	0.23
	118	perpendicular	0.51	0.19	0.32
	119	perpendicular	0.51	0.17	0.34
1000°C	124	parallel	0.57	0.16	0.41
32 hours	125	parallel	0.57	0.19	0.38
	126	perpendicular	0.59	0.19	0.40
	127	perpendicular	0.59	0.17	0.42
1100°C	132	parallel	0.18	0.23	-0.05
	133	parallel	0.18	0.17	0.01
	134	perpendicular	0.56	0.19	0.35
	135	perpendicular	0.56	0.21	0.35
1200°C	92	parallel	0.53*	0.19	0.34
8 hours	93	parallel	0.53*	0.24	0.29
	94	perpendicular	0.53*	0.20	0.33
	95	perpendicular	0.53*	0.23	0.30
1300°C	112	parallel	0.56	0.33	0.23
5 hours	113	parallel	0.56	0.30	0.26
	114	perpendicular	0.49	0.36	0.13
	115	perpendicular	0.49	0.36	0.13

*The average value of all samples is used here since no actual values are known for this group.

E. Chlorine Penetration on Exposure to NaCl Vapor

The electron probe chlorine intensities were tabulated at one and/or two micron intervals and are listed in Tables F-1 through F-20, Appendix F. Several scans had to be made on sample 119 before any chlorine penetration was detected, and the penetration detected was much greater than the other samples which were given the same treatment. Most likely the absence of detected chlorine penetration was due to a slight rounding of the sample's leading edge and a short penetration (less than 5 microns) of chlorine. Apparently the operator focused the electron beam on the higher flat surface of the sample and then moved from the sample holder onto the sample. The diffracting x-rays from the rounded edge may have not been aligned with the detector and therefore could not be observed. The excessive penetration observed in sample 119 was probably a special case where there was a small amount of general chlorine diffusion at a unique point, a crack or other defect. Samples 112, 113, 114, 115 were not polished parallel to the direction of diffusion as the other samples, because the samples broke into small fragments while cooling. Sample 112 and 113 broke parallel to the direction of diffusion and sample 114 and 115 broke only generally parallel to the direction of diffusion. The broken surfaces for samples 114 and 115 were slightly conchoidal, 115 much more than 114, and this unevenness could have caused sample 115's apparent penetration to be much greater than what actually had taken place since the sample was in effect examined at some angle other than parallel to the direction of diffusion. No difficulties were experienced with the other samples.

F. Sodium Diffusion on Exposure to NaCl Vapor

The sodium electron probe scans, Appendix G, indicated a slight amount of possible sodium diffusion. The amount of sodium diffusion was compared to that of chlorine in Table 10, and found to be small to extremely small relative to the amount of chlorine diffusion. It appeared that such a small amount of possible sodium diffusion would have had little or no effect on the chlorine diffusion rates and that the sodium effect can be considered negligible.

Table 10. Sodium Diffusion Compared to Chlorine Diffusion

Sample Number	Temperature Time	Diffusion Direction Relative to The c-axis	Amount of Diffusion Relative to Chlorine
117	900°C	parallel	very small
118	64 hours	perpendicular	very small
124	1000°C	parallel	small
126	32 hours	perpendicular	very small
133	1100°C	parallel	small
134	12 hours	perpendicular	small
93	1200°C	parallel	very small
94	8 hours	perpendicular	small
112	1300°C	parallel	extremely small
115	5 hours	perpendicular	extremely small

G. Fitting the Mathematical Model to the Chlorine Penetration Data

In Tables F-1 through F-20, Appendix F, the chlorine penetration distances versus the chlorine intensities, the relative intensities, the calculated intensities, and the differences in the calculated and relative intensities are listed. The procedure outlined in Appendix B was used to fit a mathematical model to the relative chlorine intensities and the standard error was calculated for each sample. Table 11 is a summary of the calculated standard errors. Several samples, 127, 93, 94, 95 had low error values which indicated that the mathematical model closely represented the data and diffusion process. The largest standard error was .183, sample 116, and was caused by the large fluctuations in the probe intensities.

Table 11. Standard Error for Fitted Curves

Sample Number	Standard Error	Sample Number	Standard Error	Sample Number	Standard Error
116	.183	127	.044	94	.040
117	.125	132	.121	95	.044
118	.111	133	.082	112	.142
119	.104	134	.120	113	.091
124	.082	135	.102	114	.093
125	.094	92	.062	115	.130
126	.128	93	.044		

Some of the factors which may have caused the intensities to fluctuate were the smoothness of the surface (rough ridges block x-rays from reaching the detector), background electronic noise, changes in the electron beam spot size, changes in the vacuum in the sample chamber

(higher pressures reduce x-ray intensities), and secondary radiation. The apparent intensities may have been boosted by secondary radiation which would, in effect, extend the penetration at the leading edges and would increase the lack of fit. Standard errors of less than .10, .10 to .13, and more than .13 were considered to be excellent, good, and fair fits respectively between the mathematical model and the data. In general, the standard errors in Table 11 indicate that the mathematical model used was the correct one.

H. Diffusion Coefficients

Table 12 is a list of the diffusion coefficients calculated from the fitted equations and Figure 18 is a plot of the coefficients against the inverse absolute temperature. The diffusion coefficients of the samples 115 and 119 were larger than the other samples in the same class, 112 to 115 and 116 to 119 respectively. Sample 115 was eliminated from any further consideration because apparently the surface examined was not parallel to the direction of diffusion, and sample 119 was eliminated from consideration because the recorded penetration probably occurred under special conditions. The difference in the diffusion coefficients of samples tested under identical conditions, Table 12, could have been due to the probed surface being less than parallel to the direction of diffusion, a slight difference in the crystal chemical content and structure, and different degrees of probe beam intensity fluctuations. For the other samples no readily apparent assignable causes could be found for the differences in the diffusion coefficients. Also, no correlation could be found between the residual chlorine content,

Table 12. Diffusion Coefficients

Sample Number	Temperature	Time	Diffusion Direction Relative to c-axis	Diffusion Coefficient
116	900°C	64 hours	Parallel	$4.81 \cdot 10^{-13}$
117				$1.14 \cdot 10^{-13}$
124	1000°C	32 hours	Parallel	$2.55 \cdot 10^{-12}$
125				$2.15 \cdot 10^{-12}$
132	1100°C	12 hours	Parallel	$1.69 \cdot 10^{-12}$
133				$3.19 \cdot 10^{-12}$
92	1200°C	8 hours	Parallel	$4.93 \cdot 10^{-11}$
93				$1.81 \cdot 10^{-11}$
112	1300°C	5 hours	Parallel	$4.22 \cdot 10^{-11}$
113				$6.17 \cdot 10^{-11}$
118	900°C	64 hours	Perpendicular	$1.02 \cdot 10^{-13}$
119				$9.89 \cdot 10^{-13}$
126	1000°C	32 hours	Perpendicular	$7.61 \cdot 10^{-13}$
127				$8.18 \cdot 10^{-14}$
134	1100°C	12 hours	Perpendicular	$1.31 \cdot 10^{-12}$
135				$4.65 \cdot 10^{-13}$
93	1200°C	8 hours	Perpendicular	$2.38 \cdot 10^{-12}$
94				$2.16 \cdot 10^{-12}$
114	1300°C	5 hours	Perpendicular	$6.56 \cdot 10^{-12}$
115				$6.23 \cdot 10^{-11}$

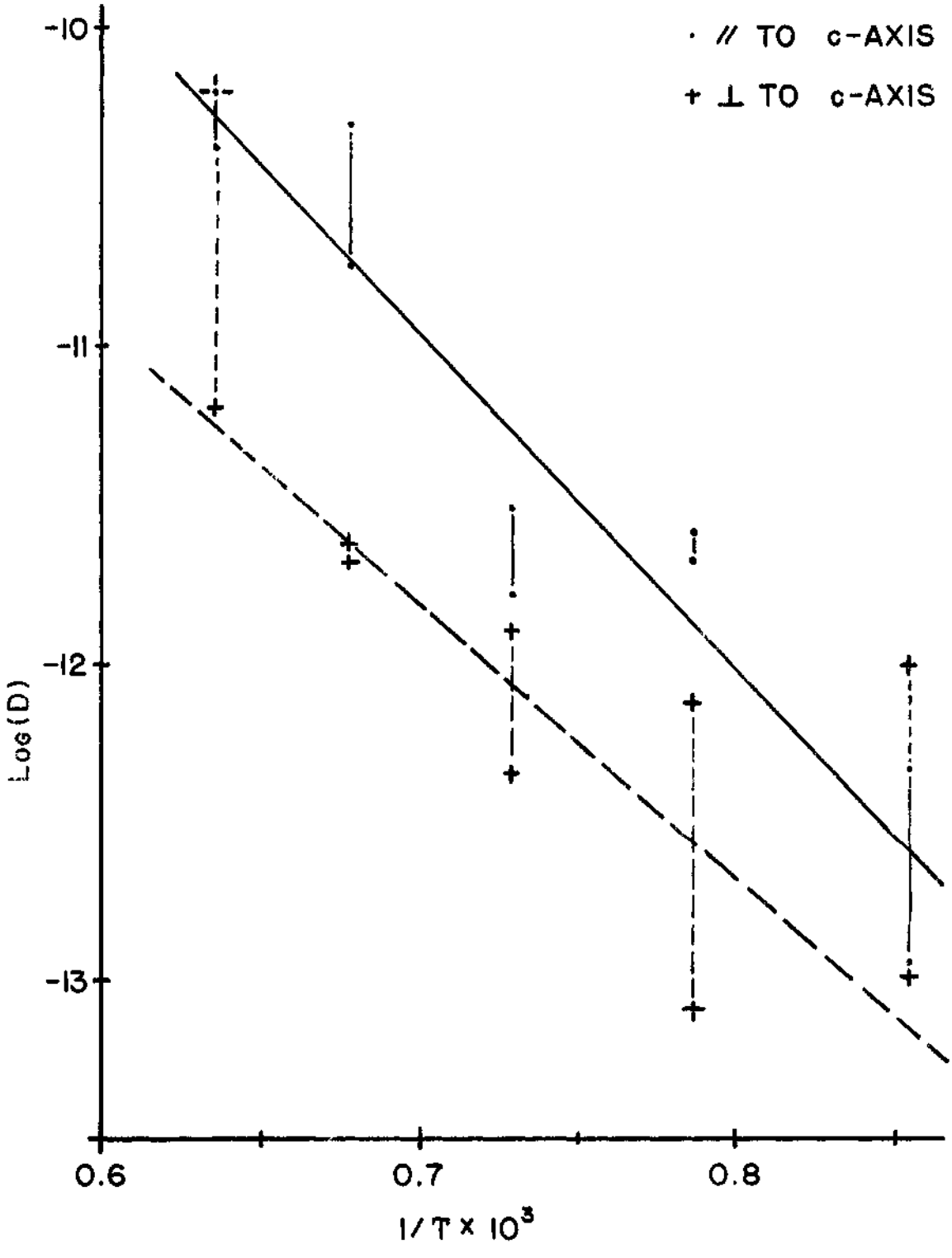

Figure 18. Log(D) vs 1/T.

Table 11, and the diffusion coefficients.

I. Activation Energy

In Figure 18 the spread of the diffusion coefficient values for the diffusion perpendicular to the c-axis in the lower temperature range suggested that there may be two linear relationships present; a larger slope relationship in the high temperature range and a smaller slope relationship in the lower temperature range. Strain and impurities may have aided the anion movement in the lower temperature test which could have been responsible for such a change in the slope on reaching the higher temperature test. However, a spread in the coefficient values caused by random errors could have increased the possibility of having an apparent multi-linear relationship when none actually existed. While a break in the slope of the plot of log (D) versus 1/T for diffusion perpendicular to the c-axis could have possibly existed, it appeared that the scatter of the data points made it difficult to justify any change in slope and that a single straight line was the best fit for the data. Also, it appeared that the data points for diffusion parallel to the c-axis followed a single linear relationship.

In Table 13 the apparent activation energy for the diffusion parallel and perpendicular to the c-axis is given with the associated 95 per cent confidence limits. The two values are not significantly different, however, some small difference should exist since structural and bonding arrangements are different in each of the directions, parallel and perpendicular to the c-axis. It appeared that the activation energies calculated were in the range of energies found for vacancy mechanisms,

Table 4, and the chlorine anions could have diffused by means of the vacancy mechanism.

Table 13. Activation Energy

Direction of Diffusion	Activation Energy
parallel to the c-axis	2.1 ± .6 electron volts
perpendicular to the c-axis	1.7 ± .8 electron volts

J. Diffusion Constants

The calculated diffusion constants are given in Table 14 with the approximate 95 per cent confidence limits. Figure 18 indicated that there was an apparent difference in the diffusion constants since the diffusion constant may be structure sensitive. The diffusion constant values were small as compared to the ideal value, Zenner (19), of 0.001 to 10 $cm^2/sec.$, this was particulary true for the constant for diffusion perpendicular to the c-axis. Probably the smaller diffusion constant was the result of short circuit diffusion paths, Zenner (19), and it was possible that the lower temperature measurements could have been influenced by the strain and impurities being released. The diffusion down the c-axis appeared to be much less influenced by possible short circuit diffusion paths as the associated diffusion constant was close to 0.001 $cm^2/sec.$ There appeared to be no correlation between the residual chlorine content in the samples, Table 9, and the diffusion constant.

Table 14. Diffusion Constants

Direction of Diffusion	Diffusion Constant, D_o
parallel to the c-axis	$3.22 \cdot 10^{-4\pm2}$ $cm^2/sec.$
perpendicular to the c-axis	$2.07 \cdot 10^{-6\pm4}$ $cm^2/sec.$

K. Diffusion Paths for Anions

Diffusion Down the Calcium Triangular Columns

Several possible diffusion paths and mechanisms for the anions, OH^-, F^-, and Cl^-, were examined. The first path was the diffusion of anions down the calcium triangular columns at the corner of the unit cell. Since the calcium columns were parallel to the c-axis, diffusion of anions in a single crystal would be expected to be highly anisotropic. OH^- and F^- anions with smaller ionic radius could have moved through a calcium triangle with less distortion of the lattice than Cl^-. The F^- anion would most likely have had the least distortion of the lattice because of its smaller size. The strength of the bonds between an anion and the neighboring calcium was most likely the rate determining factor for the diffusion of these anions, since these bonds had to be broken and remade during a diffusion step. Possibly, fluorine had the strongest bonds with the calcium triangles since it has a more electronegative character than chlorine and hydroxyl anions. Breitmoser and Young (14) reported that fluorine could not be removed from an apatite under conditions which enabled them to remove chlorine and hydroxyl anions from an apatite. If the diffusion path of the anions were down the calcium

triangular columns, the results of Breitmoser and Young could suggest that the fluorine anions had a higher bond energy than either chlorine or hydroxyl anions, and that the bonding energies of the chlorine and hydroxyl anions were about the same.

One likely method by which the anions could have moved down the calcium columns was the vacancy mechanism. Another possibility was a crowdion type of mechanism, where an extra anion was found in the calcium triangular column. The extra anion could have pushed its next like atom in the column out of its position and have occuppied that position. The displaced atom would have became an interstitial atom thus ending one cycle of the crowdion mechanism. The likelihood of finding extra anions in the calcium columns was difficult to access. The amount of vacancies present in a heated sample could have been significant at high temperatures. Normally, it is expected that the amount of anion vacancies present would increase with temperature. The release of an impurity, such as CO^2, or F could have been responsible for the appearance of new anion vacancies. The experimentally determined activation energy of 2.1 ± .6 e.v. for diffusion down the calcium columns was in the range of energies found for a vacancy mechanism as shown in Table 4, and appeared to be significantly higher than the approximate 0.5 e.v. reported by Seitz (21) for a crowdion mechanism. It appeared that the most likely diffusion mechanism that could have operated to allow anions to move along the calcium triangular columns was a vacancy mechanism.

Diffusion in Non-Column Directions

A close examination of Figure 1 indicated that there were some relatively open regions through the apatite structure which were

not parallel to the c-axis. The passages could have allowed a diffusing anion to move in directions other than in the calcium columns. The smaller OH^- and F^- anions moving in these paths would have distorted the apatite lattice less than the larger Cl^- anion, but bonding energies were expected to be the rate determining factor as to which anion moved the easier. Another factor which favored the non-column anion movement was the presence of discrete PO_4^{3-} tetrahedra and an apparent open structure as reported by Baddiel and Berry (6).

Atoms could have possibly moved through the non-column paths by a vacancy, a two-atom ring, or an interstitialcy mechanism. Vacancies in the PO_4^{3-} tetrahedra could have enabled the diffusing anions to move into unfilled oxygen positions along the non-column paths. There were probably enough vacancies present to make this a strong possibility as the main mechanism. In a two-atom ring mechanism, two atoms, a diffusing anion and an oxygen, interchanging places in the relatively open spaces of the non-column paths could have allowed the diffusing anion to move in non-column directions. This mechanism would have required more energy than the vacancy mechanism and the interstitialcy mechanism, and it appeared that this mechanism was the least likely mechanism in terms of energy requirements. The energy required for an interstitialcy mechanism was probably less than the two-atom ring mechanism and more than the vacancy mechanism. In an interstitialcy mechanism. a diffusing anion could have displaced an oxygen, forcing the displaced oxygen into interstitial regions. Another oxygen could have displaced the diffusing anion, thus forcing the anion into the interstitial region of the non-column paths, and ending one cycle of the mechanism.

The experimentally determined activation energy of 1.7 ± .8 e.v. for diffusion perpendicular to the c-axis was in the range of energies found for vacancy mechanisms in Table 4. The 1.7 ± .8 e.v. may or may not have been in the range of energies for an interstitialcy mechanism. The crystals had an apparent loss of some CO_2, Table E-4, Appendix E, which could have been a source of vacancies. It appeared that the most likely mechanism by which the chlorine anions could have diffused in the non-column directions was a vacancy mechanism. However, the interstitialcy mechanism was not eliminated as a possible mechanism.

Calcium Column Blocking by Fluorine

The activation energies for diffusion in both directions, perpendicular and parallel to the c-axis, were found to be about the same which suggested that the fluorine anions were blocking the movement of the chlorine down the calcium columns. If the chlorine movement down the calcium columns was blocked by fluorine, the energy barrier of the blocking fluorine in the calcium column could have been equal to the barrier of non-column directions, or relatively slow moving fluorine ions could have limited the rate at which the faster moving chlorine anions could have traveled down the calcium columns such that the apparent column energy barrier was equal to the non-column energy barrier. It appeared that the fluorine did have some mobility since some fluorine was found to be emitted in the mass spectrographic analysis. Probably there was some blocking of the chlorine movement in the calcium columns by fluorine, and the most likely chlorine movement process appeared to be a limited movement down the c-axis and an equal movement in non-column directions.

CHAPTER VI

CONCLUSIONS AND RECOMMENDATIONS

Conclusions

1. For small concentrations, the order of magnitude for the diffusion coefficient of chlorine through Durango, Mexico Fluorapatite can apparently be experimentally determined by using the electron probe scan and fitting a model mathematical equation to it.

2. The equation for the coefficient of diffusion of chlorine through the Durango, Mexico Fluorapatite in the direction parallel to the c-axis was determined to be:

$$D = 3.22 \cdot 10^{-4} \exp(-2.1/kT)$$

3. The equation for the coefficient of diffusion of chlorine through the Durango, Mexico Fluorapatite in the direction perpendicular to the c-axis was determined to be:

$$D = 2.07 \cdot 10^{-6} \exp(-1.7/kT)$$

4. The activation energy calculated from experimental data on diffusion of chlorine through the Durango, Mexico Fluorapatite in the direction parallel to the c-axis was 2.1 ± .6 electron volts, and in the direction perpendicular to the c-axis was 1.7 ± .8 electron volts.

5. It appears that the most likely basic mechanism for diffusion of chlorine through the Durango, Mexico Fluorapatite was of the atom-

vacancy interchange type.

6. In all probability the relatively small diffusion constant, $2.07 \cdot 10^{-6}$ $cm^2/sec.$, was the result of short circuit diffusion paths present in the direction perpendicular to the c-axis.

7. The apparent insignificant difference between the activation energies in the parallel and perpendicular directions to the c-axis suggest that the fluorine may be limiting the movement of chlorine down the clacium triangles parallel to the c-axis.

Recommendations

It is recommended that diffusion data for fluorine, hydroxyl, and chlorine anions in hydroxy and chlorapatite be obtained as it would help to verify this experimental work.

APPENDICES

APPENDIX A

CRYSTAL WAFER TEST CONDITIONS

Table A-1. Time-Temperature-Kiln Conditions

Temperature Degrees Centigrade	Time of Test in Hours	Kiln Used
900	64	Electric
1000	32	Electric
1100	12	Gas
1200	8	Gas
1300	5	Gas

APPENDIX B

LEAST SQUARE FIT PROGRAM

The Program's Function

The program took the data points and attempted to fit a curve in the form of equation (4) to the data. The fitted curve was the best equation (4) estimate of the data. The estimate was found by adjusting a constant which reduces the sum of squares to zero or a minimum. The constant is given by

$$\text{Constant} = (4Dt)^{-\frac{1}{2}} \qquad \text{(B-1)}$$

where D = diffusion coefficient

and t = elapsed time.

Once the best estimate was obtained, the constant value was solved for the value D, since all other quantities were known.

Mathematical Development of the Estimate

Mathematical Model

The mathematical model used was

$$f(X,B) = C/C_o = 1 - \text{erf}((X)(B)) \qquad \text{(B-2)}$$

where X = penetration distance

and B is an estimate of $(4Dt)^{-\frac{1}{2}}$

Equation (B-2) can be derived from equation (4) by a substitution and a rearrangement of terms where X was the independent variable,

f(X,B) was the dependent variable, and B was the estimated constant.

Error Function (erf(Z))

An approximation of the error function was used in the program. The approximation used was:

$$\text{erf}(Z) = 1 - (c_1 p + c_2 p^2 + c_3 p^3 + c_4 p^4 + c_5 p^5)(e^{-Z^2}) + E(Z) \qquad \text{(B-3)}$$

where $c_1 = 0.254829592$

$c_2 = -0.284496736$

$c_3 = 1.421413741$

$c_4 = -1.453152027$

$c_5 = 1.061405429$

$p = 1/(1 + (0.3275911(Z))$

$E(Z) = \pm 1.5 \cdot 10^{-7}$

Sum of Squares

The generated value, $f(X_i,B)$, was subtracted from the actual value, Y_i and the difference squared. The sum of the squared differences was a measure of how well the generated value agreed with the actual value. The smaller the value of the sum, the better the agreement or fit. The sum, "sum of squares," is usually denoted by SS, and the equation for the calculation of the sum of squares was:

$$SS = \sum_{i=1}^{i=n} (Y_i - f(X_i,B))^2 . \qquad \text{(B-4)}$$

If a perfect fit exists between generated function and the data, the sum

of squares will equal zero.

Standard Error

The standard error is a measure of the lack of fit between the data and the fitted function. The standard error is given by the equation:

$$\text{Standard Error} = (\text{SS}/\text{Number of data points} - 1)^{\frac{1}{2}}. \quad \text{(B-5)}$$

The smaller the standard error value, the better fit or agreement of the calculated value with the actual value.

Search Technique

The best B value was found by examining the SS response surface in small steps. The B constant was allowed to take on a range of values near an estimated best B value in small increments, and the SS calculated for each point. The value of B associated with the least SS value was selected as the best estimater of the true value of B, and was used to calculate the diffusion coefficient.

Program Outline

The general sequence of events was as follows:

1. The SS was calculated at 0.00002 steps over a 0.08 range of B.
2. The SS calculated at each step was compared to a reserve sum of squares, RSS, to see if the newly calculated value was less than the RSS, if so then RSS takes on the numerical value of SS.
3. The SS value was then stored in a two dimensional array and the value of B increased. The process was repeated until

the complete range of possible B values was covered.

4. After the range of the B values was covered, each SS value generated was evaluated to determine if it was equal to the final RSS value.
5. If an SS value was found equal to the final RSS value then the constant B associated with the SS was printed, the actual and calculated independent variables and the difference between the two were printed. The standard error and diffusion coefficient were calculated and printed.
6. When all of the array values were examined, RSS was assigned a large value and the data for the next calculation was accepted. The entire process was then repeated until all data sets had been evaluated.

APPENDIX C

CALCULATION OF E_a AND D_o

Calculation Method

The activation energy, E_a, and the diffusion constant, D_o, were found by obtaining a least square fit for the linear equation, equation (3),

$$\ln(D) = -E_a/kT + \ln(D_o), \tag{C-1}$$

by letting C_1 and C_2 be constants, X be an independent variable, and Y be a dependent variable such that

$$C_1 = \ln(D_o) \tag{C-2}$$

$$C_2 = -E_a/kT \tag{C-3}$$

$$X = 1/T \tag{C-4}$$

$$Y = \ln(D) \tag{C-5}$$

on substituting C_1, C_2, X, and Y in equation (C-1)

$$Y = C_1 + C_2X. \tag{C-6}$$

Estimates of the constants C_1 and C_2, C_1' and C_2' respectively, were found such that

$$C_1' = (\text{Sum of } Y's)/N - C_2'(\text{Sum of } X's)/N \tag{C-7}$$

$$C_2' = \frac{(\text{Sum of XY's}) - \frac{(\text{Sum of X's})(\text{Sum of Y's})}{N}}{(\text{Sum of } X^2\text{'s}) - \frac{(\text{Sum of X's})^2}{N}} \qquad \text{(C-8)}$$

where N = number of data points.

Equations (C-5) and C-6) are the normal equations for the linear equation, equation (C-5), and were used to calculate the best least square estimate of the data; the estimating equation is

$$Y' = C_1' + C_2'X. \qquad \text{(C-9)}$$

The residual, R, was the error or the difference between the actual value, Y, less the calculated value, Y'.

The standard errors for the estimators C_1' and C_2' are

$$S.E._1 = \frac{(SXS)^{\frac{1}{2}}(SRS/N)^{\frac{1}{2}}}{(N(SXS-SSX/N))^{\frac{1}{2}}} \qquad \text{(C-10)}$$

$$S.E._2 = \frac{(SRS/N)^{\frac{1}{2}}}{(SXS-SSX/N)^{\frac{1}{2}}} \qquad \text{(C-11)}$$

where: $S.E._{1,2}$ = standard error of C_1' or C_2'

SRS = sum of the squared residuals

SXS = sum of X^2's.

SSX = the square of the sum of X's

N = number of data points.

The confidence limits of C_1' and C_2' were found such that:

$$\text{limits of } C' = C' \pm (\text{S.E.})(t_{.95,v}) \qquad \text{(C-12)}$$

where: C' = estimators C_1' or C_2'

S.E. = standard error of C_1' or C_2'

$t_{.95,v}$ = the number of standard deviations for a student-t distribution with N-2 degrees of freedom at 95 per cent probability.

Numerical Example

For the diffusion parallel to the c-axis, the following data was used to calculate E_a and D_o:

$$N = 9; \qquad \frac{\text{Sum of Y's}}{N} = -26.11591 \ \ln(\text{cm}^2/\text{sec.});$$

$$\frac{\text{Sum of X's}}{N} = (7.364)10^{-4}\text{K}^{-1};$$

$$\text{Sum of XY's} = 0.193766 \ \text{K}^{-1} \ \ln(\text{cm}^2/\text{sec.})$$

$$\frac{\text{Sum of X}^2\text{'s}}{N} = (5.4228)10^{-6}\text{K}^{-2};$$

$$\frac{(\text{Sum of X})(\text{Sum of Y})}{N} = .192318 \ \text{K}^{-1} \ \ln(\text{cm}^2/\text{sec.})$$

The estimates of C_1 and C_2 were found using equations (C-7) and (C-8).

$$C_2' = \frac{-.193766 + .192318}{(5.4818 - 54228)10^{-6}}$$

$$= \frac{-.001448}{(0.059)10^{-6}}$$

$$= (-2.45423)10^4 K^{-1}$$

$$C_1' = -26.11591 - (-2.45423)(10^4)(0.7364)(10^{-3})$$

$$= -8.04296 \ln(cm^2/sec.)$$

E_a was found using equation (C-3).

$$-E_a/K = (-2.45423$$

$$E_a = \frac{(2.45423)10^4}{(1.36 \cdot 10^{-16} \text{ erg/K})(1.6 \cdot 10^{-12} \text{ erg/ev})}$$

$$= 2.1 \text{ ev}$$

D_o was found using equation (C-2).

$$\ln(D_o) = -8.04296 \ln(cm^2/sec.)$$

$$\log (D_o) = \frac{-8.04296}{2.3024} = -3.49314 = 6.50686 - 10 \log(cm^2/sec)$$

$$D_o = 3.22 \cdot 10^{-4} \text{ cm}^2/\text{sec.}$$

The estimating equation was found using equation (C-9).

$$Y' = -8.04296 - (2.45423)X$$

The sum of residuals squared divided by N-2 was found to be .55714.

The standard errors were found using equations (C-10) and (C-11).

$$S.E._1 = \frac{((5.4818)10^{-6})^{\frac{1}{2}}(.55714)^{\frac{1}{2}}}{((54.818 - 54.228)10^{6})^{\frac{1}{2}}} = \frac{17.45 \cdot 10^{4}}{7.68 \cdot 10^{-4}}$$

$$S.E._1 = 2.28 \ \ln(cm^2/sec)$$

$$S.E._2 = \frac{(.55714)^{\frac{1}{2}}}{((54.818 - 54.22)10^{5}} = \frac{7.465 \cdot 10^{-1}}{2.43 \cdot 10^{-4}}$$

$$S.E._2 = 3.07 \cdot 10^{3} \cdot K^{-1}$$

The confidence limits for C_1' and C_2' were found using equation (C-12).

$$t_{.95,8} = 2.306$$

$$\text{limits of } C_1' = -8.04296 \pm (2.306)(2.28)$$

$$= -8.04296 \pm 5.25$$

$$\text{limits of } C_2' = (-2.45423)10^{4} \pm (2.306)(3.07 \cdot 10^{3})$$

$$= (-2.45423)10^{4} \pm 7.05 \cdot 10^{3}$$

The confidence limits of E_a were found using equation (C-3).

$$\text{limits of } E_a = 2.1 \pm \frac{(7.05)10^{3}}{(1.36 \cdot 10^{-16})(1.6 \cdot 10^{-12})}$$

$$= 2.1 \pm .6 \text{ ev}$$

The approximate confidence limits for D_o were found using equation (C-2).

$$\begin{aligned}
\text{limits of } D_o &= \ln^{-1}(-8.04296 \pm 5.25) \\
&= \log^{-1}(-3.49314 \pm 2.28) \\
&= \log^{-1}(-5.77) \text{ to } \log^{-1}(-2.21) \\
&= (1.7)10^{-6} \text{ to } (6.2)10^{-3} \\
&= \text{approximately } (3.22)10^{-4\pm2} \text{ cm}^2/\text{sec.}
\end{aligned}$$

APPENDIX D

DENSITY, OPTICAL, CHEMICAL, AND X-RAY DATA

Table D-1. Densities of Several Durango, Mexico, Fluorapatite Samples

Sample	Density gr/cc	Sample	Density gr/cc
1	3.21	11	3.22
2	3.22	12	3.23
3	3.22	13	3.23
4	3.22	14	3.23
5	3.22	15	3.22
6	3.22	16	3.22
7	3.23	17	3.21
8	3.22	18	3.21
9	3.21	19	3.21
10	3.23	20	3.22

Table D-2. Densities of Some Apatites

Apatite	Density
Holly Springs Hydroxyapatite	3.11 gr./c.c.
Synthetic Chlorapatite	3.09 gr./c.c.

Table D-3. Chlorine Content of the Durango, Mexico Fluorapatite Samples

Per Cent Chlorine	Sample
0.57	A
0.56	B
0.47	C
0.50	D
0.49	E
0.53	F
0.50	G
0.51	H
0.49	I
0.50	J
0.51	K
0.57	L
0.59	M
0.56	N
0.50	O

Table D-4. Durango, Mexico Fluorapatite
X-Ray Diffraction Spectra

Spacing of Planes in Angstroms	Relative Intensity	Plane Miller Indices
8.15	11	100
5.265	7	101
4.702	7	110
4.069	9	200
3.884	9	111
3.500	7	201
3.438	44	002
3.168	15	102
3.075	17	210
2.807	100	211
2.777	35	112
2.712	65	300
2.626	30	202
2.525	9	301
2.293	7	212
2.258	24	310
2.225	7	221
2.145	7	311
2.062	7	113
1.998	7	203
1.940	33	222
1.887	13	312
1.866	4	320
1.839	61	213
1.801	20	321
1.775	13	410
1.751	13	402,303
1.721	13	004,411
1.641	9	322,223
1.608	4	313
1.584	4	301,204

Table D-5. Index of Refraction For Durango, Mexico Fluorapatite Heated to 1200°C

Indices of Refraction	Birefringence	Sign
N_e = 1.633 ± .001	-.004 ± .002	Uniaxial, negative
N_o = 1.637 ± .001		

Table D-6. Durango, Mexico Fluorapatite Heated to 1200°C, X-Ray Diffraction Spectra

Spacing of Planes in Angstroms	Relative Intensity	Plane Miller Indices
8.12	10	100
5.245	6	101
4.684	6	110
4.057	10	200
3.875	8	111
3.497	4	201
3.435	60	002
3.162	17	102
3.069	21	210
2.801	100	211
2.772	50	112
2.706	40	300
2.624	27	202
2.519	6	301
2.289	8	212
2.253	23	310
2.210	6	221
2.141	8	311
2.061	6	113
1.997	6	203
1.937	19	222
1.884	15	312
1.863	8	320
1.837	35	213
1.798	17	321
1.773	13	410
1.749	17	402,303
1.720	15	004,411
1.639	10	322,223
1.607	6	313
1.583	4	501, 204

APPENDIX E

MASS SPECTROMETER ANALYSIS OF THE DURANGO, MEXICO FLUORAPATITE DATA

Table E-1. Mass Intensities

Temperature C°	Masses 2	12	14	15	16	17	18
25	-	-	-	-	0.2	1.2	8
70	0.6	-	0.2	0.2	0.6	9	28
120	1.1	0.4	0.3	0.3	0.6	10	33
180	1.0	0.2	0.2	0.2	1.0	12	40
250	1.2	0.3	0.3	0.4	1.1	16	54
320	1.8	0.3	0.3	0.6	2.0	27	103
370	2.4	0.4	0.4	0.6	7	52	166
430	2.5	0.4	0.4	0.6	7	51	156
500	1.6	0.4	0.4	0.4	2.6	31	105
550	1.4	0.4	0.4	0.4	1.9	22	75
620	1.2	0.4	0.2	0.4	1.8	20	71
680	1.2	0.4	0.2	0.3	1.8	20	72
730	1.1	0.4	0.3	0.3	1.6	19	67
780	1.0	0.4	0.2	0.2	1.4	16	60
830	1.1	0.4	0.3	0.2	1.2	15	51
960	1.4	0.5	0.3	0.4	1.4	12	40
1080	1.2	0.5	0.4	0.4	1.5	13	46
1180	2.3	0.5	0.4	0.4	1.8	15	56
1320	4.3	0.6	0.6	0.6	2.4	20	71
1430	6.1	0.8	0.6	0.6	2.6	20	72

Table E-2. Mass Intensities

Temperature C°	Masses 19	20	26	27	28	29	30
25	-	-	-	0.2	0.8	0.2	-
70	-	-	0.2	0.4	7	0.4	0.2
120	-	-	0.3	0.6	20	1.0	0.4
180	-	-	0.2	0.7	14	0.8	0.3
250	0.2	0.2	0.4	1.0	21	1.0	0.2
320	0.2	0.2	0.4	1.0	24	1.3	0.4
370	0.4	0.4	0.4	1.2	20	1.4	0.4
430	0.4	0.4	0.4	1.0	22	1.2	0.3
500	0.2	0.3	0.4	0.8	23	1.0	0.4
550	0.2	0.2	0.3	0.7	20	0.8	0.2
620	-	0.2	0.2	0.7	29	0.8	0.2
680	0.2	0.2	0.2	0.6	20	0.8	0.3
730	0.2	0.2	0.2	0.6	18	0.8	0.2
780	0.2	0.2	0.2	0.6	20	0.8	0.2
830	0.2	0.2	0.2	0.6	17	0.8	0.2
960	-	0.2	0.6	0.9	23	0.9	0.4
1080	0.2	0.3	0.6	0.8	21	1.0	0.2
1180	0.2	0.3	0.6	1.0	20	1.1	0.4
1320	0.3	0.4	0.9	1.3	27	1.6	0.6
1430	0.2	0.7	0.8	1.2	31	1.2	0.5

Table E-3. Mass Intensities

Temperature C°	Masses 31	32	33	34	35	36	37
25	-	0.2	-	-	-	-	-
70	0.2	0.6	-	-	-	-	-
120	0.3	0.4	-	-	-	-	-
180	0.3	0.4	-	-	-	-	-
250	0.2	0.4	-	-	-	-	-
320	0.4	0.4	-	-	-	-	0.2
370	0.4	0.9	-	-	-	-	0.2
430	0.3	0.8	-	-	-	-	-
500	0.2	0.4	-	-	-	-	-
550	0.2	0.4	-	-	-	-	-
620	0.2	0.4	-	0.2	-	-	-
680	0.2	0.4	-	-	-	-	-
730	0.2	0.5	-	-	-	-	-
780	0.2	0.4	-	-	-	-	-
830	0.2	0.4	-	-	-	-	-
960	0.2	1.0	0.2	0.3	-	0.6	-
1080	0.2	1.5	0.6	1.3	0.2	0.6	0.2
1180	0.2	1.6	0.8	2.0	-	0.4	-
1320	0.5	2.2	1.4	3.1	-	0.8	0.2
1430	0.6	1.8	0.9	2.2	0.3	1.2	0.2

Table E-4. Mass Intensities

Temperature C°	Masses 38	39	40	41	42	43	44
25	-	-	-	0.2	-	0.2	-
70	-	0.4	-	0.5	0.2	0.4	0.6
120	-	0.6	-	0.8	0.6	0.6	0.9
180	-	0.5	0.2	1.0	0.4	0.6	0.8
250	0.2	0.6	0.2	1.0	0.6	0.8	1.0
320	0.2	0.6	0.2	1.2	0.5	1.0	1.6
370	0.2	0.8	0.3	1.5	0.6	1.0	2.2
430	0.2	0.6	0.3	1.2	0.6	0.8	2.5
500	-	0.6	0.2	0.8	0.4	0.8	1.8
550	-	0.4	0.2	0.9	0.4	0.5	1.6
620	0.2	0.4	-	0.8	0.4	0.5	1.3
680	0.2	0.4	-	0.8	0.4	0.5	1.6
730	0.2	0.4	-	0.7	0.4	0.6	1.6
780	0.2	0.4	-	0.7	0.4	0.5	1.5
830	-	0.4	-	0.7	0.3	0.5	1.4
960	0.4	0.6	0.2	0.8	0.7	0.6	6
1080	0.3	0.6	0.2	1.0	0.4	0.7	8
1180	0.2	0.6	0.3	1.0	0.6	0.8	7
1320	0.4	0.8	0.4	1.3	0.6	1.0	13
1430	0.6	0.6	0.3	1.2	0.7	0.8	12

Table E-5. Mass Intensities

Temperature C°	Masses 45	46	48	55	56	57	58
25	0.3	-	-	-	-	-	-
70	0.2	-	-	0.4	0.3	0.2	-
120	0.2	-	-	0.8	0.4	0.4	-
180	0.2	-	-	0.8	0.6	0.4	-
250	0.3	-	-	0.9	0.6	0.3	-
320	0.4	0.2	-	0.8	0.6	0.4	0.2
370	0.2	0.2	-	0.8	0.7	0.5	0.2
430	0.2	-	-	0.6	0.6	0.4	0.2
500	0.2	-	-	0.8	0.6	0.4	-
550	0.2	-	-	0.7	0.4	0.4	-
620	-	-	-	0.4	0.4	0.4	-
680	0.2	-	-	0.6	0.4	0.3	-
730	0.2	-	-	0.6	0.5	0.4	-
780	0.2	-	-	0.6	0.4	0.2	-
830	0.2	-	-	0.4	0.3	0.2	-
960	0.2	-	-	0.6	0.4	0.4	-
1080	0.2	-	0.6	0.5	0.5	0.4	-
1180	0.3	-	0.6	0.6	0.4	0.4	-
1320	0.2	0.2	0.5	1.0	0.8	0.4	0.4
1430	0.2	-	-	0.8	0.5	0.4	-

Table E-6. Mass Intensities

Temperature C°	Masses 60	62	64	70	78
25	-	-	-	-	-
70	-	-	-	-	0.3
120	-	-	-	-	-
180	-	-	-	0.3	0.4
250	-	-	-	0.6	-
320	-	-	-	0.3	1.1
370	-	-	-	-	-
430	-	-	-	0.2	1.2
500	-	-	-	0.2	0.8
550	-	-	-	-	0.8
620	-	-	-	-	0.7
680	-	-	-	-	0.6
730	-	-	-	-	0.6
780	-	-	-	-	0.5
830	-	-	-	-	0.4
960	-	-	-	-	0.5
1080	0.2	-	1.2	-	0.5
1180	0.2	-	1.0	-	0.6
1320	-	0.8	1.0	0.2	1.0
1430	0.2	0.8	0.4	0.4	0.8

APPENDIX F

TABULATION OF ELECTRON PROBE ANALYSIS OF CHLORINE PENETRATION INTO THE DURANGO, MEXICO FLUORAPATITE AND FITTED EQUATION CALCULATIONS

Table F-1. Sample Number 116 Chlorine Probe Intensities Compared With Calculated Values

Distance From Edge in Microns	Intensity I Counts/sec	Adjusted Intensities $I-I_o = C$	Relative Intensities $C/I_m - I_o$	Calculated Relative Intensities	Difference (RI - CRI)
3	$2700=I_m$	2100	1.0000	1.0000	.0000
4	1900	1300	.6190	.8318	-.2128
5	1250	650	.3095	.6710	-.3615
6	1150	550	.2619	.5240	-.2621
7	1050	450	.2143	.3956	-.1813
8	1500	900	.4286	.2883	.1403
9	1500	900	.4286	.2026	.2260
10	1300	700	.3333	.1371	.1962
11	1200	600	.2857	.0893	.1964
12	850	250	.1190	.0559	.0631
13	750	150	.0714	.0337	.0377
14	700	100	.0476	.0195	.0281
15	800	200	.0952	.0108	.0843
16	$600=I_o$	0	.0000	.0058	-.0058

Table F-2. Sample Number 119 Chlorine Probe Intensities Compared With Calculated Values

Distance From Edge in Microns	Intensity I Counts/sec	Adjusted Intensities $I-I_o = C$	Relative Intensities $C/I_m - I_o$	Calculated Relative Intensities	Difference (RI - CRI)
6	$1850=I_m$	1250	1.0000	1.0000	.0000
7	1500	900	.7200	.8823	-.1623
8	1500	900	.7200	.7671	-.0471
9	1250	650	.5200	.6568	-.1368
10	1400	800	.6400	.5536	.0864
11	1250	650	.5200	.4590	.0610
12	1200	600	.4800	.3742	.1058
13	850	250	.2000	.2999	-.0999
14	1100	400	.3200	.2361	.0839
15	900	300	.2400	.1826	.0574
16	$600=I_o$	0	.0000	.1386	-.1386

Table F-3. Sample Number 117 Chlorine Probe Intensities Compared With Calculated Values

Distance From Edge In Microns	Intensity I Counts/sec	Adjusted Intensities $I-I_o = C$	Relative Intensities $C/I_m - I_o$	Calculated Relative Intensities	Difference (RI - CRI)
4	$1850=I_m$	1350	1.0000	1.0000	.0000
5	1300	800	.5926	.6631	-.0705
6	900	400	.2926	.3837	-.0874
7	800	300	.2222	.1913	.0309
8	750	250	.1852	.0815	.1037
10	840	340	.2519	.0089	.2429
12	900	400	.2936	.0005	.2931
14	500	0	.0000	.0000	.0000
16	650	150	.1111	.0000	.1111
18	600	100	.0741	.0000	.0741
20	600	100	.0741	.0000	.0741
22	650	150	.1111	.0000	.1111
24	900	400	.2963	.0000	.2963
26	600	100	.0741	.0000	.0741
28	650	150	.1111	.0000	.1111
30	650	150	.1111	.0000	.1111
32	670	170	.1259	.0000	.1259
34	660	160	.1185	.0000	.1185
36	530	30	.0222	.0000	.0222
38	510	10	.0074	.0000	.0074
40	380	-120	-.0889	.0000	-.0889
42	490	-10	-.0074	.0000	-.0074
44	540	40	.0296	.0000	.0296
46	$500=I_o$	0	.0000	.0000	.0000

Table F-4. Sample Number 118 Chlorine Probe Intensities Compared With Calculated Values

Distance From Edge in Microns	Intensity I Counts/sec	Adjusted Intensities $I-I_o = C$	Relative Intensities $C/I_m - I_o$	Calculated Relative Intensities	Difference (RI - CRI)
1	$2000=I_m$	1400	1.0000	1.0000	.0000
2	1550	950	.6786	.6444	.0342
3	1150	550	.3928	.3559	.0369
4	700	100	.0714	.1661	-.0947
5	590	-10	-.0071	.0648	-.0719
6	800	200	.1429	.0210	.1219
7	900	300	.2143	.0056	.2087
8	1000	400	.2858	.0012	.2846
9	900	300	.2143	.0002	.2141
10	690	90	.0643	.0000	.0642
11	500	-100	-.0714	.0000	-.0714
12	510	-90	-.0643	.0000	-.0643
13	700	100	.0714	.0000	.0714
14	600	0	0	.0000	.0000
15	550	-50	-.0357	.0000	-.0357
16	500	-100	-.0714	.0000	-.0714
17	520	-80	-.0471	.0000	-.0571
18	520	-80	-.0571	.0000	-.0571
19	780	180	.1286	.0000	.1286
20	520	-80	-.0571	.0000	-.0571
21	770	170	.1214	.0000	.1214
22	520	-80	-.0571	.0000	-.0571
23	$600=I_o$	0	.0000	.0000	.0000

Table F-5. Sample Number 124 Chlorine Probe Intensities Compared With Calculated Values

Distance From Edge in Microns	Intensity I Counts/sec	Adjusted Intensities $I-I_o = C$	Relative Intensities $C/I_m - I_o$	Calculated Relative Intensities	Difference (RI - CRI)
2	$1900=I_m$	1450	1.0000	1.0000	.0000
3	1700	1250	.8625	.8961	-.0336
4	1550	1100	.7586	.7940	-.0354
5	1550	1100	.7586	.6953	.0633
6	1400	950	.6552	.6015	.0537
7	1100	650	.4483	.5139	-.0656
8	1300	850	.5862	.4334	.1528
9	1150	700	.4828	.3608	.1220
10	850	400	.2759	.2963	-.0204
11	500	50	.0345	.2400	-.2055
12	550	100	.0690	.1917	-.1227
13	590	140	.0966	.1510	-.0544
14	620	170	.1172	.1172	.0000
15	660	210	.1448	.0896	.0552
16	485	35	.0241	.0676	-.0435
17	520	70	.0483	.0502	-.0019
18	590	140	.0966	.0367	.0599
19	800	350	.2414	.0265	.2149
20	510	60	.0414	.0188	.0226
21	510	60	.0414	.0131	.0283
22	450	0	.0000	.0090	-.0090
23	510	60	.0414	.0061	.0353
24	440	-10	-.0069	.0041	-.0010
25	445	-5	.0035	.0027	-.0062
26	440	-10	-.0069	.0017	-.0086
27	$400=I_o$	0	.0000	.0011	-.0011

Table F-6. Sample Number 126 Chlorine Probe Intensities Compared With Calculated Values

Distance From Edge in Microns	Intensity I Counts/sec	Adjusted Intensities $I-I_o = C$	Relative Intensities $C/I_m - I_o$	Calculated Relative Intensities	Difference (RI - CRI)
2	$2950=I_m$	2400	1.0000	1.0000	.0000
3	2300	1750	.7292	.8112	-.0820
4	2900	2350	.9792	.6329	.3463
5	2400	1850	.7708	.4737	.2971
6	1000	450	.1875	.3394	-.1519
7	550	0	0	.2324	-.2324
8	600	50	.0208	.1519	-.1311
9	800	250	.1042	.0946	.0096
10	520	-30	-.0125	.0560	-.0685
11	720	170	.0708	.0316	.0392
12	720	170	.0708	.0169	.0539
13	620	70	.0292	.0086	.0206
14	550	0	0	.0042	-.0042
15	650	100	.0417	.0019	.0398
16	700	150	.0625	.0008	.0617
17	560	10	.0042	.0003	.0039
18	560	10	.0042	.0001	.0041
19	500	-50	-.0208	.0000	-.0285
20	530	-20	-.0083	.0000	-.0083
21	620	70	.0292	.0000	.0292
22	$550=I_o$	0	.0000	.0000	.0000

Table F-7. Sample Number 133 Chlorine Probe Intensities Compared With Calculated Values

Distance From Edge in Microns	Intensity I Counts/sec	Adjusted Intensities $I-I_o = C$	Relative Intensities $C/I_m - I_o$	Calculated Relative Intensities	Difference (RI - CRI)
4	$2750=I_m$	2150	1.0000	1.0000	.0000
5	2400	1800	.8372	.8489	-.0117
6	2200	1600	.7442	.7031	.041
7	1600	1000	.4651	.5675	-.1024
8	2000	1400	.6512	.4459	.2053
9	1400	800	.3721	.3406	.0315
10	750	150	.0698	.2528	-.1836
11	800	200	.0930	.1822	-.0892
12	1000	400	.1860	.1274	.0586
13	950	350	.1628	.0863	.0765
14	660	0	.0000	.0567	-.0567
15	700	100	.0465	.0360	.0105
16	750	150	.0698	.0222	.0476
17	600	0	.0000	.0132	-.0132
18	750	150	.0698	.0076	.0622
19	700	100	.0465	.0043	.0422
20	750	150	.0698	.0023	.0675
21	750	150	.0698	.0012	.0686
22	500	-100	-.0465	.0006	-.0471
23	$600=I_o$	0	.0000	.0003	-.0003

Table F-8. Sample Number 134 Chlorine Probe Intensities Compared With Calculated Values

Distance From Edge in Microns	Intensity I Counts/sec	Adjusted Intensities $I-I_o = C$	Relative Intensities $C/I_m - I_o$	Calculated Relative Intensities	Difference (RI - CRI)
1	$1400=I_m$	800	1.0000	1.0000	.0000
2	1200	600	.7500	.7666	-.0166
3	1100	500	.6250	.5527	.0723
4	830	230	.2875	.3732	-.0857
5	800	200	.2500	.2351	.0149
6	700	100	.1250	.1378	-.0128
7	650	50	.0625	.0749	-.0124
8	550	-50	-.0625	.0377	-.1002
9	750	150	.1875	.0176	.1699
10	700	100	.1250	.0075	.1175
11	800	200	.2500	.0030	.2470
12	750	150	.1875	.0011	.1864
13	750	150	.1875	.0004	.1871
14	650	50	.0625	.0001	.0624
15	$600=I_o$	0	.0000	.0000	.0000

Table F-9. Sample Number 125 Chlorine Probe Intensities Compared With Calculated Values

Distance From Edge in Microns	Intensity I Counts/sec	Adjusted Intensities $I-I_o = C$	Relative Intensities $C/I_m - I_o$	Calculated Relative Intensities	Difference (RI - CRI)
5	$3050=I_m$	2500	1.0000	1.0000	.0000
6	2800	2250	.9000	.8870	.0130
7	2600	2050	.8200	.7762	.0438
8	2400	1950	.7800	.6698	.1102
9	2350	1800	.7200	.5695	.1504
10	2150	1600	.6400	.4772	.1628
11	1650	1100	.4400	.3940	.0463
12	1560	950	.3800	.3197	.0603
13	850	300	.1200	.2554	-.1354
14	800	250	.1000	.2008	-.1008
15	780	230	.0920	.1552	-.0632
16	480	-70	-.0280	.1179	-.1459
17	560	10	.0040	.0880	-.0840
18	700	150	.0600	.0646	-.0056
19	630	80	.0320	.0466	-.0146
20	$550=I_o$	0	.0000	.0330	-.0330

Table F-10. Sample Number 135 Chlorine Probe Intensities Compared With Calculated Values

Distance From Edge in Microns	Intensity I Counts/sec	Adjusted Intensities $I-I_o = C$	Relative Intensities $C/I_m - I_o$	Calculated Relative Intensities	Difference (RI- CRI)
1	$2150=I_m$	1850	1.0000	1.0000	.0000
2	1800	1500	.8108	.6179	.1929
3	600	300	.1622	.3185	-.1563
4	600	300	.1622	.1346	.0276
5	350	50	.0270	.0460	-.0190
6	350	50	.0270	.0126	.0144
7	$300=I_o$	0	.0000	.0028	-.0028

Table F-11. Sample Number 127 Chlorine Probe Intensities Compared With Calculated Values

Distance From Edge in Microns	Intensity I Counts/sec	Adjusted Intensities $I-I_o = C$	Relative Intensities $C/I_m - I_o$	Calculated Relative Intensities	Difference (RI - CRI)
3	$2700=I_m$	2150	1.0000	1.0000	.0000
4	1650	1100	.5116	.4663	.0453
5	750	200	.0930	.1451	-.0521
6	600	50	.0233	.0288	-.0055
7	650	100	.0465	.0036	.0429
8	650	100	.0465	.0003	.0462
9	690	140	.0651	.0000	.0651
10	620	170	.0791	.0000	.0791
11	410	-110	-.0512	.0000	-.0512
12	485	-65	-.0302	.0000	-.0302
13	700	150	.-698	.0000	.0698
14	600	50	.0233	.0000	.0233
15	480	-70	-.0326	.0000	-.0326
16	550	0	.0000	.0000	.0000
17	570	20	.0093	.0000	.0093
18	$550=I_o$	0	.0000	.0000	.0000

Table F-12. Sample Number 94 Chlorine Intensities Compared With Calculated Values

Distance From Edge in Microns	Intensity I Counts/sec	Adjusted Intensities $I-I_o = C$	Relative Intensities $C/I_m - I_o$	Calculated Relative Intensities	Difference (RI - CRI)
2	$2600=I_m$	2000	1.0000	1.0000	.0000
3	2300	1700	.8500	.7871	.0629
4	1900	1300	.6500	.5892	.0608
5	1400	800	.4000	.4179	-.0179
6	1200	600	.3000	.2801	.0199
7	900	300	.1500	.1770	-.0270
8	750	150	.0750	.1052	-.0302
9	$600=I_o$	0	.0000	.0000	.0000

Table F-13. Sample Number 92 Chlorine Probe Intensities Compared With Calculated Values

Distance From Edge in Microns	Intensity I Counts/sec	Adjusted Intensities $I-I_o = C$	Relative Intensities $C/I_m - I_o$	Calculated Relative Intensities	Difference (RI - CRI)
5	$2500=I_m$	2100	1.0000	1.0000	.0000
6	2450	2050	.9762	.9527	.0235
7	2200	1800	.8571	.9055	-.0484
8	2250	1850	.8810	.8587	.0229
9	2100	1700	.8095	.8124	-.0288
10	2350	1950	.9286	.7667	.1619
11	1700	1300	.6190	.7218	-.1028
12	2100	1700	.8095	.6779	.1316
13	1600	1200	.5714	.6350	-.0636
14	1800	1400	.6667	.5933	.0734
15	1900	1500	.7143	.5529	.1614
16	1600	1200	.5714	.5139	.0575
17	1400	1000	.4762	.4764	-.0002
18	1300	900	.4286	.4405	-.0119
19	1300	900	.4286	.4061	.0225
20	1300	900	.4286	.3734	.0552
21	1300	900	.4286	.3424	.0862
22	1100	700	.3333	.3131	.0202
23	1000	600	.2857	.2755	.0002
24	850	450	.2143	.2595	-.0452
25	800	400	.1905	.2353	-.0448
26	700	300	.1429	.2127	-.0698
27	780	380	.1810	.1917	-.0107
28	650	250	.1190	.1723	-.0533
29	650	250	.1190	.1544	-.0354
30	570	170	.0810	.1379	-.0569
31	600	200	.0952	.1229	-.0277
32	570	170	.0810	.1091	-.0281
33	570	170	.0810	.0966	-.0156
34	500	100	.0476	.0853	-.0377
35	500	100	.0476	.0750	-.0274
36	450	50	.0238	.0658	-.0420
37	400	0	.0000	.0576	-.0576
38	430	30	.0143	.0502	-.0359
39	500	100	.0476	.0436	-.0040
40	$400=I_o$	0	.0000	.0378	-.0378

Table F-14. Sample Number 93 Chlorine Probe Intensities Compared With Calculated Values

Distance From Edge in Microns	Intensity I Counts/sec	Adjusted Intensities $I-I_o = C$	Relative Intensities $C/I_m - I_o$	Calculated Relative Intensities	Difference (RI - CRI)
5	$3125=I_m$	2775	1.0000	1.0000	.0000
6	2750	2500	.9009	.9219	-.0210
7	2500	2150	.7748	.8445	-.0697
8	3350	1900	.6847	.7686	-.0839
9	2100	1750	.6306	.6949	-.0643
10	2150	1800	.6486	.6239	.0247
11	1850	1500	.5405	.5563	-.0158
12	1750	1400	.5045	.4924	.0121
13	1625	1275	.4595	.4328	.0267
14	1375	1025	.3694	.3775	-.0081
15	1375	1025	.3694	.3268	.0426
16	1125	775	.2793	.2807	-.0014
17	875	525	.1892	.2393	-.0501
18	1000	650	.2342	.2024	.0318
19	1000	650	.2342	.1698	.0644
20	700	350	.1261	.1413	-.0152
21	625	272	.0990	.1167	-.0177
22	625	275	.0990	.0955	.0035
23	575	225	.0811	.0775	.0036
24	500	150	.0541	.0624	-.0083
25	250	-100	-.0360	.0499	-.0859
26	625	275	.0990	.0395	.0595
27	375	25	.0090	.0310	-.0220
28	750	400	.1441	.0241	.0120
29	350	0	.0000	.0186	-.0186
30	475	125	.0450	.0142	.0308
31	450	100	.0360	.0108	.0252
32	355	5	.0018	.0081	-.0063
33	375	25	.0090	.0060	.0030
34	$350=I_o$	0	.0000	.0045	-.0045

Table F-15. Sample Number 132 Chlorine Probe Intensities Compared With Calculated Values

Distance From Edge in Microns	Intensity I Counts/sec	Adjusted Intensities $I-I_o = C$	Relative Intensities $C/I_m - I_o$	Calculated Relative Intensities	Difference (RI - CRI)
6	$2200=I_m$	1850	1.0000	1.0000	.0000
7	1250	900	.4865	.7938	-.3073
8	1100	750	.4054	.6011	-.1957
9	1400	1050	.5676	.4376	.1347
10	850	500	.2703	.2957	-.0254
11	850	500	.2703	.1912	.0791
12	700	350	.1892	.1168	.0724
13	600	250	.1351	.0673	.0678
14	400	50	.0270	.0365	-.0095
15	450	100	.0541	.0186	.0355
16	450	100	.0541	.0089	.0452
17	250	-100	-.0541	.0040	-.0581
18	$350=I_o$	0	.0000	.0017	-.0017

Table F-16. Sample Number 95 Chlorine Probe Intensities Compared With Calculated Values

Distance From Edge in Microns	Intensity I Counts/sec	Adjusted Intensities $I-I_o = C$	Relative Intensities $C/I_m - I_o$	Calculated Relative Intensities	Difference (RI - CRI)
5	$3200=I_m$	2600	1.0000	1.0000	.0000
6	2600	2000	.7692	.7770	-.0078
7	2000	1400	.5385	.5710	-.0325
8	1700	1100	.4231	.3954	.0277
9	1275	675	.2596	.2571	.0025
10	1000	400	.1538	.1566	-.0028
11	600	0	.0000	.0892	-.0892
12	1000	400	.1538	.0474	.1064
13	700	100	.0385	.0234	.0151
14	750	150	.0577	.0107	.0469
15	620	20	.0077	.0046	.0031
16	620	20	.0077	.0018	.0059
17	$600=I_o$	0	.0000	.0005	-.0005

Table F-17. Sample Number 112 Chlorine Probe Intensities Compared With Calculated Values

Distance From Edge in Microns	Intensity I Counts/sec	Adjusted Intensities $I-I_o = C$	Relative Intensities $C/I_m - I_o$	Calculated Relative Intensities	Difference (RI - CRI)
4	$2650=I_m$	2200	1.0000	1.0000	.0000
5	2250	1800	.8182	.9353	-.1171
6	2250	1800	.8182	.8711	-.0529
7	1600	1150	.5227	.8077	-.2850
8	1400	950	.4318	.7456	-.3138
9	1350	900	.4091	.6850	-.2759
10	1300	850	.3864	.6265	-.2401
11	1250	800	.3636	.5701	-.2065
12	1250	800	.3636	.5164	-.1528
13	1200	750	.3409	.4653	-.1244
14	1250	800	.3636	.4173	-.0536
15	1250	800	.3636	.3722	-.0086
16	1150	700	.3183	.3303	-.0121
17	1200	750	.3409	.2916	.0493
18	750	300	.1364	.2561	-.1197
19	1100	650	.2955	.2237	.0718
20	1400	950	.4318	.1943	.2375
21	1550	1100	.5000	.1679	.3321
22	1350	900	.4091	.1442	.2649
23	900	450	.2045	.1233	.0812
24	650	200	.0909	.1047	-.0138
25	600	150	.0682	.0885	-.0203
26	800	350	.1591	.0743	.0848
27	1000	550	.2500	.0621	.1879
28	900	450	.2045	.0516	.1529
29	800	350	.1591	.0426	.1165
30	600	150	.0682	.0349	.0333
31	550	100	.0455	.0285	.0170
32	650	200	.0909	.0213	.0678
33	700	250	.1136	.0186	.0950
34	450	0	.0000	.0150	-.0150
35	600	150	.0682	.0119	.0563
36	500	50	.0227	.0094	.0133
37	600	150	.0682	.0074	.0608
38	550	100	.0455	.0058	.0397
39	450	0	.0000	.0045	-.0045
40	400	-50	-.0227	.0035	-.0262
41	500	50	.0227	.0027	.0200
42	400	-50	-.0227	.0021	-.0248
43	$450=I_o$	0	.0000	.0016	-.0016

Table F-18. Sample Number 113 Chlorine Probe Intensities Compared With Calculated Values

Distance From Edge in Micron	Intensity I Counts/sec	Adjusted Intensities $I-I_o = C$	Relative Intensities $C/I_m - I_o$	Calculated Relative Intensities	Difference (RI - CRI)
0	$3100=I_m$	2350	1.0000	1.0000	.0000
1	2750	2000	.8511	.9465	-.0954
2	2450	1700	.7234	.8923	-.1699
3	2300	1550	.6596	.8405	-.1809
4	1900	1150	.4894	.7884	-.2990
5	2300	1550	.7234	.7373	-.0139
6	2000	1250	.5319	.6873	-.1554
7	1900	1150	.4894	.6387	-.1492
8	2250	1500	.6383	.5915	.0468
9	1900	1150	.4894	.5460	-.0566
10	1850	1100	.4681	.5081	-.0342
11	1700	950	.4043	.4605	-.0562
12	1500	750	.3191	.4208	-.1017
13	1750	1000	.4255	.3855	.0424
14	1600	850	.3617	.3476	.0141
15	1500	750	.3191	.3142	.0049
16	1500	750	.3191	.2831	.0360
17	1500	750	.3191	.2541	.0650
18	1350	600	.2553	.2272	.0281
19	1300	550	.2340	.2024	.0316
20	1225	475	.2021	.1797	.0224
21	1240	500	.2128	.1589	.0539
22	1200	450	.1915	.1399	.0516
23	1500	750	.3191	.1228	.1963
24	1150	400	.1702	.1074	.0628
25	1225	475	.2021	.0935	.1086
26	1000	250	.1064	.0811	.0253
27	875	125	.0532	.0701	-.0169
28	1050	300	.1277	.0603	.0674
29	900	150	.0638	.0517	.0121
30	850	100	.0426	.0441	-.0015
31	850	100	.0426	.0375	.0051
32	800	50	.0213	.1318	-.0105
33	750	0	.0000	.0268	-.0268
34	800	50	.0213	.0225	-.0012
35	750	0	.0000	.0189	-.0189
36	850	100	.0426	.0157	.0269
37	$750=I_o$	0	.0000	.0131	-.0131

Table F-19. Sample Number 114 Chlorine Probe Intensities Compared With Calculated Values

Distance From Edge in Micron	Intensity I Counts/sec	Adjusted Intensities $I-I_o = C$	Relative Intensities $C/I_m - I_o$	Calculated Relative Intensities	Difference (RI - CRI)
8	$3800=I_m$	3200	1.0000	1.0000	.0000
9	3700	3100	.9688	.8373	.1315
10	2900	2300	.7188	.6813	.0375
11	2700	2100	.6563	.5379	.1184
12	1800	1200	.3750	.4115	-.0365
13	1700	1100	.3438	.3046	.0392
14	800	200	.0625	.2180	-.1555
15	700	100	.0313	.1507	-.1194
16	575	-25	-.0078	.1005	-.1083
17	800	200	.0625	.0646	-.0021
18	1000	400	.1250	.0401	.0849
19	1250	650	.2031	.0239	.1792
20	1100	500	.1563	.0137	.1426
21	1200	600	.1875	.0076	.1799
22	1100	500	.1563	.0040	.1523
23	1100	500	.1563	.0021	.1542
24	650	50	.0156	.0010	.0146
25	550	-50	-.0156	.0005	-.0161
26	500	-100	-.0313	.0002	-.0315
27	600	0	.0000	.0001	-.0001
28	775	175	.0547	.0000	.0547
29	700	100	.0313	.0000	.0313
30	750	150	.0469	.0000	.0469
31	700	100	.0313	.0000	.0310
32	625	25	.0078	.0000	.0078
33	700	100	.0313	.0000	.0313
34	575	-25	-.0078	.0000	-.0078
35	$600=I_o$	0	.0000	.0000	.0000

Table F-20. Sample Number 115 Chlorine Probe Intensities Compared With Calculated Values

Distance From Edge in Microns	Intensity I Counts/sec	Adjusted Intensities $I-I_o = C$	Relative Intensities $C/I_m - I_o$	Calculated Relative Intensities	Difference (RI - CRI)
0	$4500=I_m$	3800	1.0000	1.0000	.0000
1	4000	3300	.8684	.9468	-.0784
2	3600	2900	.7631	.8940	-.1307
3	3300	2600	.6842	.8413	-.1571
4	3900	3200	.8421	.7895	.0526
5	3600	2900	.7631	.7386	.0245
6	2800	2100	.5526	.6888	-.1362
7	2700	2000	.5263	.6403	-.1140
8	2500	1800	.4737	.5933	-.1196
9	2300	1600	.4210	.5480	-.1270
10	2400	1700	.4474	.5044	-.0570
11	2500	1800	.4737	.4628	.0109
12	2700	2000	.5263	.4231	.1032
13	2100	1400	.3684	.3855	-.0171
14	2300	1600	.4210	.3500	.0710
15	3000	2300	.6052	.3167	.2885
16	3100	2400	.6316	.2855	.3461
17	2300	1600	.4210	.2565	.1645
18	2100	1400	.3684	.2296	.1388
19	1900	1200	.3158	.2047	.1111
20	1150	450	.0658	.1819	-.1161
21	700	0	.0000	.1610	-.1610
22	700	0	.0000	.1420	-.1420
23	800	100	.0263	.1247	-.0984
24	1000	300	.0789	.1092	-.0303
25	750	50	.0132	.0952	-.0820
26	850	150	.0395	.0826	-.0431
27	650	-50	-.0132	.0715	-.0849
28	700	0	.0000	.0616	-.0616
29	750	50	.0132	.0529	-.0397
30	$700=I_o$	0	.0000	.0452	-.0452

APPENDIX G

TABULATION OF ELECTRON PROBE ANALYSIS

OF SODIUM PENETRATION INTO THE DURANGO, MEXICO FLUORAPATITE

Table G-1. Sample Number 117 Sodium Probe Intensities

Distance From Edge in Microns	Intensities Counts/sec	Distance From Edge in Microns	Intensities Counts/sec
0	1000	7	350
1	400	8	200
2	400	9	250
3	750	10	250
4	600	11	250
5	350	12	250
6	500		

Table G-2. Sample Number 118 Sodium Probe Intensities

Distance From Edge in Microns	Intensities Counts/sec	Distance From Edge in Microns	Intensities Counts/sec
0	300	4	100
1	200	5	80
2	200	6	20
3	50	7	15

Table G-3. Sample Number 124 Sodium Probe Intensities

Distance From Edge in Microns	Intensities Counts/sec	Distance From Edge in Microns	Intensities Counts/sec
0	270	6	150
1	230	7	150
2	200	8	130
3	170	9	110
4	140	10	100
5	150		

Table G-4. Sample Number 126 Sodium Probe Intensities

Distance From Edge in Microns	Intensities Counts/sec	Distance From Edge in Microns	Intensities Counts/sec
0	490	5	150
1	350	6	140
2	200	7	100
3	180	8	100
4	170	9	120

Table G-5. Sample Number 133 Sodium Probe Intensities

Distance From Edge in Microns	Intensities Counts/sec	Distance From Edge in Microns	Intensities Counts/sec
0	1500	7	500
1	1000	8	800
2	750	9	700
3	1000	10	800
4	750	11	750
5	700	12	650
6	300		

Table G-6. Sample Number 134 Sodium Probe Intensities

Distance From Edge in Microns	Intensities Counts/sec	Distance From Edge in Microns	Intensities Counts/sec
0	1100	4	350
1	500	5	300
2	500	6	300
3	500		

Table G-7. Sample Number 93 Sodium Probe Intensities

Distance From Edge in Microns	Intensities Counts/sec	Distance From Edge in Microns	Intensities Counts/sec
0	750	5	600
1	650	6	350
2	750	7	300
3	450	8	200
4	450		

Table G-8. Sample Number 94 Sodium Probe Intensities

Distance From Edge in Microns	Intensities Counts/sec	Distance From Edge in Microns	Intensities Counts/sec
0	1000	6	500
1	750	7	450
2	600	8	550
3	700	9	400
4	650	10	300
5	700	11	300

Table G-9. Sample Number 112 Sodium Probe Intensities

Distance From Edge in Microns	Intensities Counts/sec	Distance From Edge in Microns	Intensities Counts/sec
0	800	5	500
1	400	6	500
2	400	7	450
3	500	8	300
4	350	9	350

Table G-10. Sample Number 115 Sodium Probe Intensities

Distance From Edge in Microns	Intensities Counts/sec	Distance From Edge in Microns	Intensities Counts/sec
0	1500	5	800
1	750	6	650
2	650	7	650
3	900	8	650
4	900	9	500

BIBLIOGRAPHY

1. R. C. Evans, An Introduction to Crystal Chemistry, 2nd ed.; pp. 39,139. Cambridge University Press, Cambridge, 1966.

2. A. S. Posner, A. Perloff, and A. F. Diorio, "Refinement of the Hydroxyapatite Structure," Acta Crystallographica, 11, 308 (1958).

3. M. I. Kay, R. A. Young, and A. S. Posner, "Crystal Structure of Hydroxyapatite," Nature, 204, 1050 (1964).

4. R. A. Young and J. C. Elliott, "Atomic-scale Bases for Several Properties of Apatites," Archs Oral Biology, 11, 699 (1966).

5. O. R. Trautz, "Crystallographic Studies of Calcium Carbonate Phosphate," Annals New York Academy of Sciences, 60, 696 (1955).

6. C. B. Baddiel and E. E. Berry, "Spectra Structure Correlations in Hydroxy and Fluorapatite," Spectrochim Acta, 22, 1407 (1966).

7. J. Bhimasenachar, "Elastic Constants of Apatite," Proceedings of the Indian Academy of Science, 22, 209 (1946).

8. D. Carlstrom, "X-ray Crystallographic Studies on Apatite and Calcified Structures," Acta Radiological Supplement 121, (1955).

9. E. S. Larson and H. Berman, Geological Survey Bulletin 848; p. 83. Department of the Interior, Washington, 1934.

10. A. Scheede, B. Meppen, and O. B. Jorgenson, "Zur Frage der Citronensaureloslichkeit von Naturphoshaten (Apatiten), Angewandte Chemie, 52, 316 (1939).

11. R. Wallaeys, "Contribution a L'etude des Apatites Phosphocaliques," Annalles Chimie, 7, 808 (1952).

12. J. C. Elliott and R. A. Young, "Conversion of Single Crystals of Chlorapatite into Single Crystals of Hydroxyapatite," Nature, 214, 904 (1967).

13. H. G. Breitmoser and R. A. Young, "A Possible Mechanism for the Cariostatic Effect of Fluorine on Teeth," Bulletin of the Georgia Academy of Science, 25, 108 (1967).

14. R. M. Barrer, Diffusion In and Through Solids, pp. 1-52; Cambridge University Press, London, 1951.

15. J. Crank, The Mathematics of Diffusion, pp. 1-8; Oxford University Press, Oxford, 1951.

16. L. S. Darken, "Formal Bases of Diffusion Theory in Atom Movements," pp. 1-25; American Society for Metals, Cleveland, 1951.

17. Barrer, op. cit., p. 274.

18. Ibid., pp. 272-305.

19. C. Zenner, "Theory of D_o for Atomic Diffusion in Metals," Journal of Applied Physics, 22, 372 (1951).

20. F. Seitz, "Mechanisms of Diffusion," in Phase Transformations in Solids, pp. 80-96; John Wiley and Sons, New York, 1951.

21. P. G. Shewmon, Diffusion in Solids, pp. 43-47; McGraw-Hill, New York, 1963.

22. B. J. Wuensch and T. Vasilos, "Diffusion of Transition Metal Ions in Single-Crystal MgO," Journal of Chemical Physics, 36, 2917 (1962).

23. B. J. Wuensch and T. Vasilos, "Diffusion in Refractory Oxides," in the Proceedings of the Fourth International Symposium on Reactivity of Solids, pp. 57-64; Elsevier Publishing Company, New York, 1961.